

MeToken: UNIFORM MICRO-ENVIRONMENT TOKEN BOOSTS POST-TRANSLATIONAL MODIFICATION PREDICTION

Cheng Tan^{1,2*}, Zhenxiao Cao^{3*}, Zhangyang Gao^{2*}, Lirong Wu², Siyuan Li², Yufei Huang², Jun Xia², Bozhen Hu², Stan Z. Li^{2†}

¹Zhejiang University, Hangzhou, China ³Xi'an Jiaotong University, China

²AI Lab, Research Center for Industries of the Future, Westlake University, Hangzhou, China
{tancheng, gaozhangyang}@westlake.edu.cn; alancao@stu.xjtu.edu.cn

ABSTRACT

Post-translational modifications (PTMs) profoundly expand the complexity and functionality of the proteome, regulating protein attributes and interactions that are crucial for biological processes. Accurately predicting PTM sites and their specific types is therefore essential for elucidating protein function and understanding disease mechanisms. Existing computational approaches predominantly focus on protein sequences to predict PTM sites, driven by the recognition of sequence-dependent motifs. However, these approaches often overlook protein structural contexts. In this work, we first compile a large-scale sequence-structure PTM dataset, which serves as the foundation for fair comparison. We introduce the MeToken model, which tokenizes the micro-environment of each amino acid, integrating both sequence and structural information into unified discrete tokens. This model not only captures the typical sequence motifs associated with PTMs but also leverages the spatial arrangements dictated by protein tertiary structures, thus providing a holistic view of the factors influencing PTM sites. Designed to address the long-tail distribution of PTM types, MeToken employs uniform sub-codebooks that ensure even the rarest PTMs are adequately represented and distinguished. We validate the effectiveness and generalizability of MeToken across multiple datasets, demonstrating its superior performance in accurately identifying PTM types. The results underscore the importance of incorporating structural data and highlight MeToken’s potential in facilitating accurate and comprehensive PTM predictions, which could significantly impact proteomics research. The code and datasets are available at github.com/A4Bio/MeToken.

1 INTRODUCTION

Post-translational modifications (PTMs) are chemical modifications that occur to proteins following biosynthesis (Consortium, 2004; Hanahan & Coussens, 2012), playing a pivotal role in regulating biological processes including signal transduction (Meng et al., 2022; Walsh et al., 2005), protein degradation (Jensen, 2004; Craveur et al., 2019; Humphrey et al., 2015), and cellular localization (Li et al., 2021; Deribe et al., 2010). PTMs can alter the properties and functions of a protein by modifying its chemical structure, often serving as switches that toggle protein activity. The diverse nature of PTMs, which include phosphorylation, glycosylation, acetylation, ubiquitination, and methylation, reflects their varied roles across different cellular processes and conditions (Walsh & Jefferis, 2006). Given their complexity and the critical functionality they impart, accurately predicting PTM sites and their specific types is essential for elucidating protein functions, advancing therapeutic development, and unraveling the molecular bases of diseases (Cruz et al., 2019; Tsikas, 2021).

Despite their significance, predicting PTM types remains a formidable challenge due to the inherent complexity of protein structures and the subtle, context-dependent nature of modification sites. Re-

*Equal contribution.

†Corresponding author.

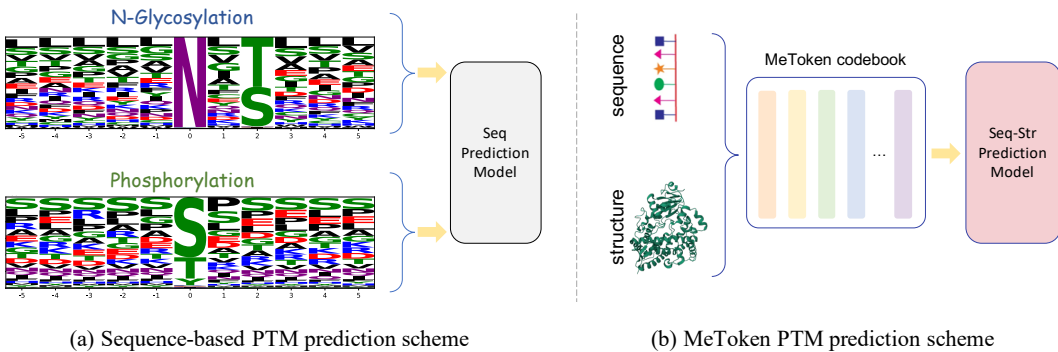


Figure 1: The comparison of sequence-based and MeToken schemes. While sequence-based methods focus on sequence motifs around modification sites, MeToken first encodes the micro-environment at both sequence and structure levels and predicts the PTM types with token embeddings.

searchers have struggled with several key difficulties: **(i) Predominant computational approaches focus on sequence-dependent motifs while neglecting tertiary structural information.** As depicted in Figure 1(a), the N-glycosylation modification exhibits a well-defined 'Asn-X-T/S' sequence motif, a finding thoroughly illustrated by (Bause & Hettkamp, 1979). However, the situation is notably more complex for phosphorylation, where the sequence motifs are less consistent and more variable. The reliance on sequence data alone limits the ability to predict PTM types. **(ii) Lack of large-scale sequence structure PTM dataset.** Though the sequence-structure co-modeling manner has been well explored in protein function prediction (Wang et al., 2022; Hermosilla et al., 2020; Zhang et al., 2022; Fan et al., 2022; Hu et al., 2023), the PTM prediction significantly lacks in terms of a comprehensive, annotated sequence-structure dataset at the residue level. **(iii) The severe long-tail distribution of PTM types.** The distribution of PTM types is highly skewed, with a few types being overwhelmingly more common than others. The lack of representation not only complicates model training with imbalanced data but also hampers the model’s generalization ability.

In this paper, we first compile a large-scale sequence-structure PTM dataset featuring over 1.2 million residue-level annotated sites across multiple PTM types. Furthermore, we introduce the MeToken (Micro-environment Token) model, which integrates both sequence and structural information from the sequence-structure pair. Recognizing that PTMs are influenced not only by the immediate sequence environment but also by the intricate spatial context, MeToken employs a micro-environment-based approach to capture comprehensive contextual information for each amino acid, thereby providing a holistic view that is critical for predicting potential PTMs.

To decipher the typical micro-environment patterns associated with PTMs, we develop a codebook that distills complex and high-dimensional data into simpler, representative tokens with distinct and meaningful representations. The codebook is constructed to learn a set of discrete tokens that correlate specifically to PTMs with minimal redundancy, ensuring that each token captures unique and interpretable information about the micro-environment. Furthermore, we propose a uniform sub-codebook strategy that effectively addresses the long-tail distribution of PTM types, which projects the PTM types into a uniformly distributed token space, ensuring that even the rarest PTMs are adequately represented and distinctly discriminated. By leveraging our tokenization strategy, MeToken not only enhances interpretability but also significantly improves its predictive performance by fine-tuning the model specifically for the PTM prediction task. We conduct extensive experiments to validate the effectiveness and generalizability of MeToken across multiple datasets, demonstrating its superior performance in accurately identifying PTM types.

The contributions of our work are summarized as:

- Recognizing the critical importance of structural context in PTM prediction, we have compiled a large-scale sequence-structure PTM dataset, which serves as the foundational basis for the PTM predictions based on sequence-structure pairs.

- In analogy to sequence motifs used in sequence-based PTM prediction, we introduce the concept of the micro-environment token. The contextual information at both the sequence and structural levels can be uniquely represented within a set of discrete tokens.
- To address the severe long-tail problem prevalent in PTM data, we have devised a codebook construction strategy that incorporates uniform sub-codebooks, ensuring that PTMs are adequately represented and distinctly discernible. Extensive experiments demonstrate the effectiveness and generalizability of MeToken in accurately predicting PTM types.

2 RELATED WORK

Post-Translation Modification Prediction Early work on PTM prediction primarily involved manually extracting sequence motifs from around potential modification sites and employing various learning-based methods for prediction (Xue et al., 2010; Lee et al., 2011; Gao et al., 2017; Jia et al., 2016a;b; Luo et al., 2019; Kirchoff & Gomez, 2022; Meng et al., 2022). For example, PPSP (Xue et al., 2006) utilized Bayesian decision theory, focusing on a motif of nine amino acids. LysAcet (Li et al., 2009) used support vector machines (SVM) and sequence coupling patterns. Other methods like PWAA introduced position weight amino acid composition encoding (Qiu et al., 2017), while LightGBM-CroSite combined binary encoding and position weight matrices (Liu et al., 2020). DeepNitro (Xie et al., 2018) incorporated positional amino acid distributions and position-specific scoring matrices. Deep-Kcr integrated sequence-based features and employed convolutional neural networks (CNN) (Lv et al., 2021). DeepSuccinylSite employed one-hot and word embeddings to enhance predictions (Thapa et al., 2020), and Adapt-Kcr combined adaptive embedding with convolutional and long short-term memory networks (LSTM), along with an attention mechanism (Li et al., 2022b). While these methods have shown effectiveness, they are limited by their reliance on sequence motifs, which cannot fully capture the intricate complexity and contextual dependencies of PTM sites. Despite efforts to integrate sequence and structural data in PTM prediction, the attempt has been largely constrained by the scarcity of comprehensive datasets (Li et al., 2024; Yan et al., 2023). The largest sequence-structure database, PRISMOID (Li et al., 2020), includes 3,919 protein structure entries with 17,145 non-redundant modification sites. In this work, we compile a large-scale sequence-structure PTM dataset with over 1.2 million annotated sites across over 180,000 proteins.

Sequence-structure Co-modeling Sequence-structure co-modeling has become a common manner in predicting protein property and function. LM-GVP (Wang et al., 2021) combined protein language model and graph neural networks (GNN) to predict protein properties from both their amino acid sequences and 3D structures. DeepFRI (Gligorijević et al., 2021) employed a similar strategy and used homology models. GearNet (Zhang et al., 2022) is a seminal work that pretraining protein representations based on 3D structures using a graph encoder and multiview contrastive learning. ProNet (Wang et al., 2022) employed a hierarchical graph network to learn detailed and granular protein representations. CDConv (Fan et al., 2022) utilized independent weights for regular sequential displacements and direct encoding for irregular geometric displacements. While these methods utilized local sequence-structure patterns to learn global protein-level properties, PTM prediction differs fundamentally as it directly employs the local sequence-structure micro-environments to predict modifications at the residue level.

Micro-environment Tokenization Vector quantization (VQ) is a pivotal technique for efficient data compression and representation. The basic premise involves compressing latent representations by mapping them to the nearest vector within a codebook. Vanilla VQ (Van Den Oord et al., 2017) straightforwardly assigns each vector in the latent space to the closest codebook vector. Product Quantization (Jégou et al., 2011; Chen et al., 2020; El-Nouby et al., 2022) segments the high-dimensional space into a Cartesian product of lower-dimensional subspaces. Residual quantization (Juang & Gray, 1982; Martinez et al., 2014; Lee et al., 2022; Zeghidour et al., 2021) iteratively quantizes vectors and their residuals, representing the vector as a stack of codes. Lookup-free VQ (Mentzer et al., 2023; Yu et al., 2023b) quantizes each dimension to a fixed set of values. Although advancements in vector quantization have shown promise in molecular modeling (Xia et al., 2022; Gao et al., 2024; Wu et al., 2024), the specific application of micro-environment tokenization in PTM prediction remains underexplored, particularly given the challenges posed by the long-tail distribution of PTMs.

3 PRELIMINARIES

A protein \mathcal{P} is composed of N amino acids, which are organized as a string of primary sequence, denoted as $\mathcal{S} = \{s_i\}_{i=1}^N$. Each element s_i within this sequence is referred to as a residue, representing one of the 20 standard amino acid types. In the real physicochemical environment of a cell, these sequences fold into stable three-dimensional structures. This three-dimensional conformation is defined by the coordinates of backbone atoms, represented as $\mathcal{X} = \{\mathbf{x}_{i,\omega}\}_{i=1}^N$, where $\mathbf{x}_{i,\omega} \in \mathbb{R}^3$ and ω encompasses the main backbone atoms, specifically $\{C\alpha, N, C, O\}$. The sequence-structure pair of a protein is represented as $\mathcal{P} = (\mathcal{S}, \mathcal{X})$.

Modeling the sequence and structure of a protein \mathcal{P} as a residue-level protein graph $\mathcal{G} = (\mathcal{V}, \mathcal{E})$ is a widely recognized approach (Tan et al., 2024; Luo et al., 2022; Kong et al., 2023a; Jin et al., 2020; Kong et al., 2023b). In this representation, \mathcal{V} represents the node embeddings, which are derived from the amino acid sequence s_i and the spatial arrangement $\{\mathbf{x}_{i,\omega} | \omega \in \{C\alpha, N, C, O\}\}$ of the backbone atoms within each residue. The edges, denoted as \mathcal{E} , encapsulate the interactions between residues, represented as edge embeddings that reflect the various types of connections. The node and edge embedding construction is detailed in the Appendix B. Building on the concept of the micro-environment, as outlined in previous works (Huang et al., 2023; Lu et al., 2022; Wu et al., 2024), the micro-environment of a residue i within \mathcal{G} is characterized by its node set $V_{\text{ME}}^i \subseteq \mathcal{V}$, can be formally defined as:

$$V_{\text{ME}}^i = \left\{ v_j \mid |i - j| \leq d_s, \|C\alpha_i - C\alpha_j\| \leq d_r, v_j \in \mathcal{N}_i^{(K)}, \forall j \right\}, \quad (1)$$

where d_s and d_r represent the cut-off distances within the sequence and in 3D space, respectively. $C\alpha_i$ and $C\alpha_j$ denote the 3D coordinates of the carbon-alpha atoms in residues i and j , and $\mathcal{N}_i^{(K)}$ indicates the K -hop neighborhood of residue i in the 3D structure.

Thus, the types of edges in the micro-environment focus on three specific interactions: (i) *sequential edge*, connecting two residues in the sequence within a cutoff distance d_s ; (ii) *radius edge*, connecting two residues if the spatial Euclidean distance between them is less than a threshold d_r ; and (iii) *K -nearest edge*, connecting two residues that are among the spatial K -nearest neighbors to each other. Consequently, the complete micro-environment of residue i is represented as $\mathcal{G}_{\text{ME}}^i = (V^i, E_{\text{ME}}^i)$, where $V^i \in \mathcal{V}$ includes the node embedding of the residue i and E_{ME}^i includes the edge embeddings connecting residue i with its neighboring nodes from three kinds of edges in the set V_{ME}^i .

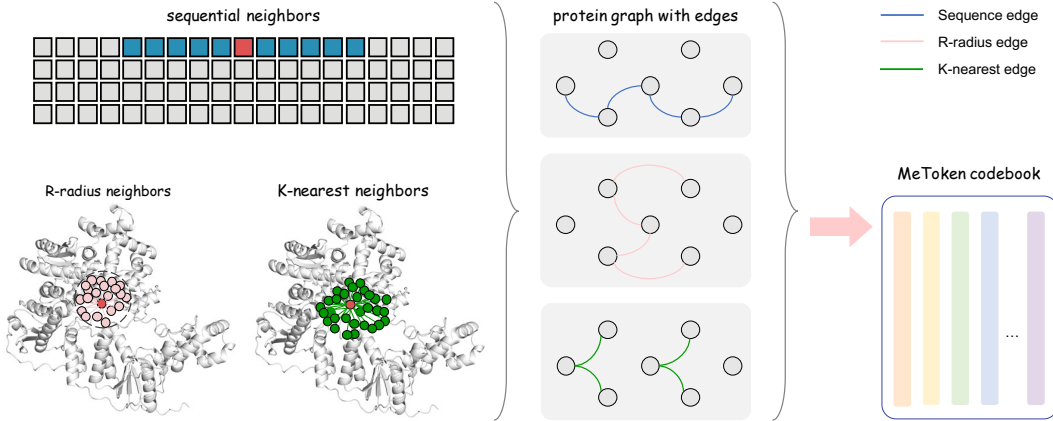


Figure 2: Illustration of the micro-environment of residue i . This figure depicts the local neighborhood of residue i , highlighted in red, which is interconnected through various types of edges: sequential edges (blue), R -radius edges (pink), and K -nearest edges (green). The entire micro-environment, including residue i and its interconnected neighbors, is then tokenized into a unified representation token for PTM prediction.

In this study, our primary objective is to effectively encode the micro-environment of each residue i within the protein graph \mathcal{G} , by seamlessly integrating crucial sequence and structural information into

a single, unified discrete token. As depicted in Figure 2, the micro-environment of residue i is adeptly tokenized into a unified representation token. The core of our tokenization process involves developing a mapping function $\mathcal{F} : \mathcal{G}_{\text{ME}}^i \rightarrow e^j$, where $e^j \in \mathbb{R}^d$ denotes a d -dimensional token embedding. This embedding is not merely a numerical representation but a rich encapsulation of the complex patterns of sequence and spatial features that characterize the unique micro-environment surrounding residue i . Here, j signifies the token index within the codebook \mathcal{C} , ranging over $[1, |\mathcal{C}|] \cap \mathbb{Z}$.

4 METOKEN

In this section, we detail the methodologies underlying our proposed MeToken model, which aims to tackle the challenges posed by the diverse nature and varying frequency of PTM types observed across different proteins. The MeToken model is specifically designed to manage the long-tail distribution of PTM types and capture subtle, yet crucial, biochemical signals in protein micro-environments.

4.1 UNIFORM SUB-CODEBOOK CONSTRUCTION

Recognizing that the distribution of PTM types exhibits a severe long-tail pattern, where many PTM types are infrequently observed, it is imperative to ensure that rare PTMs are adequately represented in the learning process. To achieve this, we allocate an identical size of sub-codebook to each PTM type, irrespective of their frequency in the dataset. This uniformity ensures that no PTM type is inherently disadvantaged by a lack of representative power within the model’s architecture.

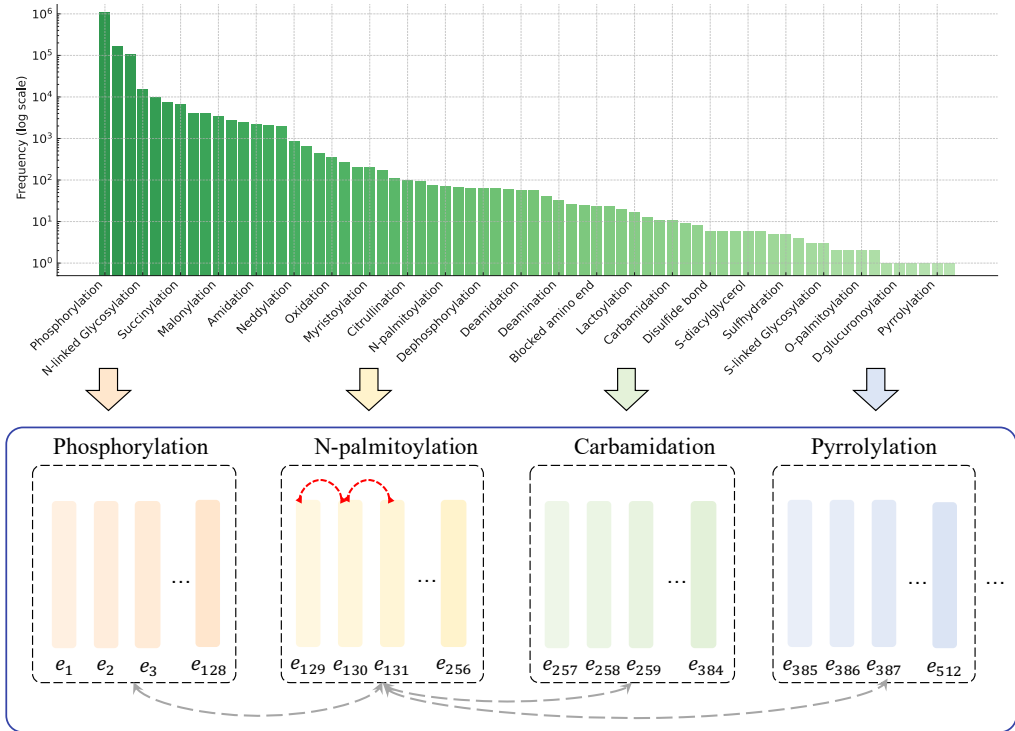


Figure 3: The long-tail distributed PTM types are projected into a uniformly distributed token space. Red arrows depict the consolidation of token embeddings within each sub-codebook, enhancing intra-class similarity. In contrast, gray arrows represent the dispersion of token embeddings across different sub-codebooks, promoting inter-class distinctiveness.

As illustrated in Figure 3, each sub-codebook is designed to capture distinct patterns that are characteristic of specific PTM types. However, merely maintaining a uniform size for each sub-codebook does not inherently prevent the potential risk of token embeddings collapsing into non-discriminative clusters. To address this, we implement a uniform loss mechanism specifically designed to refine the

distribution of token embeddings, which is formally defined as follows:

$$\mathcal{L}_u = -\frac{1}{|\mathcal{C}|} \sum_{i=1}^{|\mathcal{C}|} \log \frac{\sum_{j=1}^{|\mathcal{C}|} C_{ij} \mathbb{1}_{S_i=S_j}}{\sum_{j=1}^{|\mathcal{C}|} C_{ij}}, \quad (2)$$

where S_i denotes the PTM type of token i , $C_{ij} = \exp(\frac{e_i^T e_j}{\|e_i\| \|e_j\|} / \tau_u)$ represents the cosine similarity between tokens i and j scaled by the temperature τ_u , and $\mathbb{1}_{S_i=S_j}$ is an indicator that is 1 if token i and j share the same PTM type, and 0 otherwise. This formulation maximizes intra-class similarities, thereby enhancing the homogeneity of embeddings within each PTM class. Simultaneously, it minimizes inter-class similarities, promoting heterogeneity across different PTM types.

4.2 TEMPERATURE-SCALED VECTOR QUANTIZATION

Vanilla vector quantization (Van Den Oord et al., 2017) maps each input vector to the nearest vector in a predefined set, known as a codebook. This mapping results in a "hard assignment" that can be represented as:

$$z_i = \arg \min_j \|\mathbf{h}_i - \mathbf{e}_j\|^2, \quad (3)$$

where $\mathbf{h}_i \in \mathbb{R}^d$ represents the input vector and \mathbf{e}_j denotes the nearest codebook vector. The index z_i identifies the specific codebook vector that minimizes the Euclidean distance to \mathbf{h}_i . A fundamental limitation of this method is the non-differentiable nature of the mapping process due to the hard assignment, which relies on the nearest neighbor search. This search uses the encoder output to find the closest code, thereby rendering the quantization step non-differentiable:

$$\mathcal{L}_{vq} = \mathcal{L}_{recon} + \|\text{sg}[\mathbf{h}_i] - \mathbf{e}_{z_i}\|_2^2 + \beta \|\mathbf{h}_i - \text{sg}[\mathbf{e}_{z_i}]\|_2^2, \quad (4)$$

where \mathcal{L}_{recon} is the reconstruction loss. $\text{sg}[\cdot]$ indicates the stop-gradient operation, and β is the trade-off hyperparameter. However, the rigid and non-differentiable characteristics of hard quantization may not effectively capture the subtle and complex variations typical in PTM datasets, particularly in the context of our model which employs uniform sub-codebook construction. These challenges can lead to gradient sparsity and impede the learning process, necessitating a more flexible approach.

In our model, we implement a temperature-scaled vector quantization mechanism that introduces a temperature parameter, τ_v , to modulate the quantization process. The quantization process can be mathematically defined as follows:

$$\hat{\mathbf{h}}_i = \sum_{j=1}^{|\mathcal{C}|} a_{ij} \mathbf{e}_j, \quad a_{ij} = \frac{\exp(\mathbf{h}_i^T \mathbf{e}_j / \tau_v)}{\sum_{k=1}^{|\mathcal{C}|} \exp(\mathbf{h}_i^T \mathbf{e}_k / \tau_v)}, \quad (5)$$

where a_{ij} represents the attention weight assigned to the j -th codebook vector for the i -th input vector. These weights are computed using a softmax function, scaled by the temperature parameter τ_v , which modulates the sharpness of the resulting attention distribution. A higher τ_v leads to a more diffuse distribution across the codebook vectors, promoting a broader exploration of the vector space and mitigating the risk of premature convergence to suboptimal quantizations. Initially set at 1, τ_v is gradually reduced towards zero during training. As τ_v diminishes, a_{ij} transitions towards a one-hot distribution, rendering the quantization process increasingly deterministic. The quantization selects the codebook vector corresponding to the highest attention weight, identified by $z_i = \arg \max_j a_{ij}$. The codebook training loss incorporates both the reconstruction loss and a uniform loss:

$$\mathcal{L}_{codebook} = \mathcal{L}_{recon} + \alpha \mathcal{L}_u \quad (6)$$

where α is set as 0.1 empirically, balancing the reconstruction loss and the uniform loss.

4.3 PTM PREDICTION WITH LEARNED CODEBOOK

The learned codebook, derived from the training set, contains vectors that capture the unique attributes of protein micro-environments. As depicted in Figure 5, during the prediction phase, we extract the codebook vector \mathbf{e}_{z_i} corresponding to the quantized index z_i associated with each residue's micro-environment. This retrieval initiates the prediction process. To predict the specific PTM type for each residue, we employ a prediction network built from three layers of PiGNN (Gao et al., 2022),

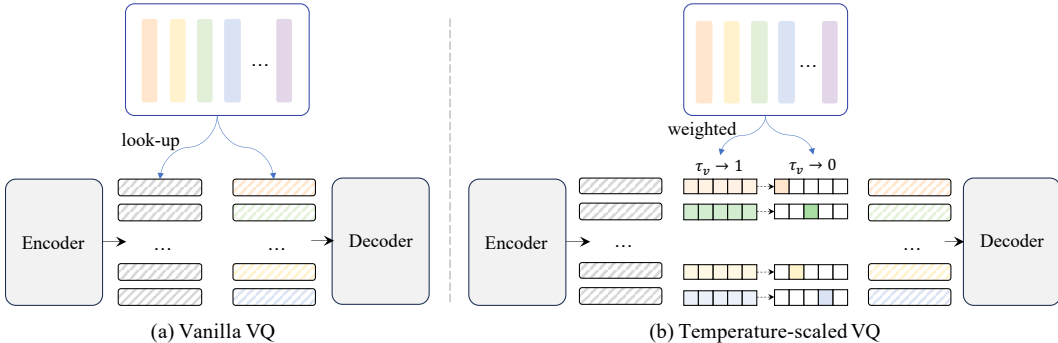


Figure 4: Vanilla VQ looks up the codebook and hard-assigns the nearest code, while temperature-scaled VQ employs a softer, probabilistic assignment approach where codebook vectors are assigned based on weights. These weights are modulated by τ_v , which adjusts the sharpness throughout the training process, transitioning from exploratory to more deterministic assignments as τ_v decreases.

a graph neural network tailored for protein graph data. This network directly processes the quantized codebook vectors e_{z_i} transforming these richly encoded representations into predictions about PTM types. The predictor network is trained using the cross-entropy loss, which is defined as:

$$\mathcal{L}_{pred} = - \sum_i \sum_c y_{ic} \log p(y_{ic} | \mathbf{h}_i), \quad (7)$$

where y_{ic} indicates whether the i -th site has the PTM type c , \mathbf{h}_i is the micro-environment embedding.

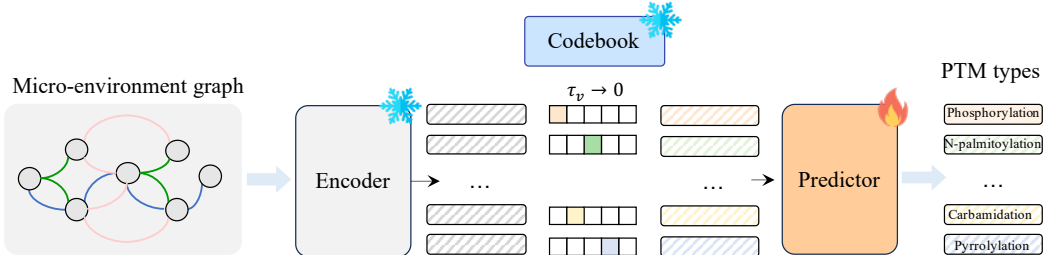


Figure 5: The PTM prediction process with the learned codebook.

5 EXPERIMENT

Datasets Experiments are conducted on three datasets: *our large-scale dataset*, *PTMint*, and *qPTM*. We constructed a large-scale dataset by integrating dbPTM (Li et al., 2022a), the most extensive sequence-based PTM dataset available, with structural data obtained from the Protein Data Bank (PDB) (Berman et al., 2000) and the AlphaFold database (Varadi et al., 2022; 2024). We utilized MMseqs2 (Steinegger & Söding, 2017) to cluster the data based on sequence similarity with a threshold of 40% and grouped the data into clusters, which were then allocated to the training, validation, or test set. Our large-scale PTM dataset with over 1.2 million annotated sites across over 180,000 proteins is the largest PTM dataset with both sequence and structure data. To assess the generalizability, we used the pre-trained models on the large-scale dataset to directly test on the PTMint (Hong et al., 2023) and qPTM (Yu et al., 2023a) datasets. The details of the dataset construction and the statistics of open-sourced datasets are outlined in Appendix C.

Baselines We compare the performance against a selection of established PTM prediction models. Specifically, we include sequence-based baselines such as EMBER (Kirchoff & Gomez, 2022), DeepPhos (Luo et al., 2019), and MusiteDeep (Wang et al., 2017). MIND (Yan et al., 2023) is a sequence-structure baseline. *In addition to these PTM-specific models, we incorporate baselines from broader protein modeling domains.* For structure-based baselines, we adapt StructGNN (Ingraham et al., 2019), GraphTrans (Ingraham et al., 2019), GVP (Jing et al., 2020), and PiFold (Gao et al., 2022), which are primarily designed for structure-based protein sequence design. Similarly, ESM-2 (Lin et al., 2023) is fine-tuned to serve as an additional sequence-based PTM predictor. Moreover,

GearNet (Zhang et al., 2022) and CDConv (Fan et al., 2022), originally designed for protein function prediction, are also adapted to act as sequence-structure co-modeling baselines.

Metrics Regarding the PTM prediction problem as a multi-class classification problem, we employed a comprehensive suite of metrics, such as accuracy, precision, recall, F1-score, MCC, AUROC, and AUPRC within our multi-class context. We detail these metrics in the Appendix D.

5.1 MeToken OUTPERFORMS BASELINE MODELS ON THE LARGE-SCALE DATASET

To evaluate the performance of MeToken, we conducted extensive tests on our large-scale dataset that incorporates both sequence and structural data. Table 1 presents the performance comparison of MeToken against a range of baseline models. It is noteworthy that both sequence-based and structure-based baselines exhibit comparable performances, each utilizing only a single modality.

Among these, the finetuned ESM-2 emerged as the most robust, achieving the best performance across all baselines. Despite its strong performance, MeToken demonstrates superior capabilities, achieving a remarkable 6.46% improvement in F1-score over ESM-2. This significant performance underscores the efficacy of MeToken in leveraging micro-environment information from sequence-structure data.

Table 1: Performance comparison on the large-scale dataset. The mean/std of three runs is reported.

Input	Method	F1-score	Accuracy	Precision	Recall	MCC	AUROC	AUPRC
Seq	EMBER	10.94 \pm 0.77	72.89 \pm 0.12	15.34 \pm 0.94	9.55 \pm 0.67	19.75 \pm 1.07	64.47 \pm 2.12	9.89 \pm 0.71
	DeepPhos	3.58 \pm 0.00	74.33 \pm 0.01	5.75 \pm 0.18	4.18 \pm 0.01	2.96 \pm 0.09	59.34 \pm 1.42	5.17 \pm 0.16
	MusiteDeep	3.55 \pm 0.00	74.18 \pm 0.06	3.09 \pm 0.00	4.17 \pm 0.00	0.00 \pm 0.00	48.85 \pm 1.04	4.01 \pm 0.01
	ESM-2	43.94 \pm 0.07	89.75 \pm 0.01	55.67 \pm 1.94	42.15 \pm 0.04	75.83 \pm 0.01	91.52 \pm 0.03	47.31 \pm 0.14
Str	StructGNN	12.86 \pm 0.06	75.62 \pm 0.08	21.16 \pm 0.61	11.06 \pm 0.18	29.73 \pm 0.26	78.94 \pm 0.46	13.51 \pm 0.18
	GraphTrans	5.03 \pm 0.49	74.14 \pm 0.11	12.23 \pm 0.72	5.12 \pm 0.40	9.87 \pm 1.82	74.75 \pm 0.08	7.99 \pm 0.27
	GVP	17.51 \pm 1.12	77.62 \pm 0.16	32.19 \pm 4.87	14.43 \pm 0.92	37.95 \pm 0.89	82.47 \pm 0.52	18.83 \pm 1.29
	PiFold	8.87 \pm 4.69	75.11 \pm 1.37	18.42 \pm 5.43	8.03 \pm 3.71	22.59 \pm 10.15	76.81 \pm 4.37	11.02 \pm 4.43
Seq + Str	GearNet	16.63 \pm 1.64	85.75 \pm 1.13	17.09 \pm 1.37	21.01 \pm 1.45	67.64 \pm 2.44	89.37 \pm 0.29	21.79 \pm 0.25
	CDConv	18.11 \pm 0.62	87.29 \pm 0.09	19.18 \pm 1.97	22.58 \pm 1.52	70.88 \pm 0.16	89.42 \pm 0.21	21.94 \pm 0.41
	MIND	26.70 \pm 0.72	86.30 \pm 0.24	33.35 \pm 4.07	25.21 \pm 0.84	66.63 \pm 0.48	77.37 \pm 1.74	22.29 \pm 0.36
	MeToken	50.40 \pm 0.06	89.91 \pm 0.05	58.08 \pm 0.38	47.93 \pm 0.14	76.03 \pm 0.06	92.20 \pm 0.03	51.26 \pm 0.14

5.2 MeToken GENERALIZE WELL ON PTMINT AND QPTM

To further evaluate the effectiveness and generalizability of MeToken, we conducted rigorous tests on two additional datasets, PTMint and qPTM, after training the models on our large-scale dataset. We refined the qPTM dataset by excluding data with sequence similarity greater than 40% compared to our training set to prevent data leakage, while the PTMint dataset remained unfiltered due to its relatively small size. The summarized results in Tables 2 and 3 highlight MeToken’s consistent superiority over all baselines across various metrics on both datasets.

The PTMint dataset, although smaller in scale, contains a well-curated collection of samples spread across several protein types, making it an ideal testbed for evaluating PTM predictions. The results from Table 2 demonstrate that MeToken significantly outperforms sequence-only and structure-only models, showcasing its capability to integrate micro-environments from complex data modalities.

On the other hand, the qPTM dataset provides a more expansive evaluation landscape due to its large volume of samples and diversity of protein types, making it perfectly suited for assessing the scalability and adaptability of PTM models. As illustrated in Table 3, MeToken not only excels in performance but also consistently achieves superior metrics across all evaluated categories when compared to competing models. The strong performance of MeToken across these varied datasets underscores its capacity to generalize well beyond the confines of its initial training environment. This trait is especially crucial in proteomics, where predictive models must reliably perform across a wide array of unseen data, encompassing diverse biological contexts and experimental conditions.

Table 2: Performance comparison on the PTMint dataset. The mean/std of three runs is reported.

Input	Method	F1-score	Accuracy	Precision	Recall	MCC	AUROC	AUPRC
Seq	EMBER	21.27 \pm 3.81	81.53 \pm 1.05	21.98 \pm 4.91	21.40 \pm 2.34	8.16 \pm 1.11	66.60 \pm 2.24	30.23 \pm 1.21
	DeepPhos	19.32 \pm 1.20	85.97 \pm 1.50	18.55 \pm 0.85	20.68 \pm 2.34	-2.00 \pm 2.99	53.64 \pm 2.06	22.66 \pm 0.79
	MusiteDeep	19.01 \pm 0.01	90.54 \pm 0.11	18.11 \pm 0.02	20.00 \pm 0.00	0.00 \pm 0.00	49.70 \pm 2.66	22.11 \pm 1.01
	ESM-2	36.46 \pm 2.23	93.07 \pm 0.59	41.78 \pm 7.87	36.30 \pm 1.05	61.50 \pm 3.41	97.79 \pm 0.09	60.82 \pm 2.02
Str	StructGNN	20.55 \pm 1.66	87.29 \pm 0.78	21.69 \pm 1.45	20.23 \pm 1.71	13.52 \pm 4.98	77.74 \pm 0.04	33.71 \pm 2.60
	GraphTrans	20.55 \pm 3.43	87.56 \pm 1.45	19.53 \pm 3.15	22.18 \pm 4.34	5.91 \pm 5.47	63.50 \pm 2.30	26.41 \pm 1.90
	GVP	25.00 \pm 4.64	87.41 \pm 1.49	25.23 \pm 4.17	26.11 \pm 5.43	29.56 \pm 6.04	76.88 \pm 1.59	33.17 \pm 0.76
	PiFold	20.32 \pm 3.28	89.19 \pm 0.15	21.54 \pm 4.76	20.59 \pm 3.05	13.28 \pm 4.21	71.02 \pm 0.89	27.73 \pm 0.83
Seq + Str	GearNet	32.09 \pm 0.24	94.31 \pm 0.16	28.66 \pm 0.25	40.00 \pm 0.00	68.23 \pm 0.55	97.69 \pm 0.12	56.47 \pm 1.32
	CDCConv	29.30 \pm 3.77	92.75 \pm 0.65	26.62 \pm 3.59	39.50 \pm 2.68	59.98 \pm 2.17	97.83 \pm 0.29	56.97 \pm 0.96
	MIND	35.04 \pm 1.49	93.25 \pm 0.58	34.07 \pm 4.53	38.46 \pm 1.32	64.40 \pm 2.25	81.30 \pm 3.50	51.56 \pm 1.19
	MeToken	42.07 \pm 1.26	94.51 \pm 0.15	38.74 \pm 0.60	49.59 \pm 1.41	70.92 \pm 1.45	98.55 \pm 0.19	73.22 \pm 2.57

Table 3: Performance comparison on the qPTM dataset. The mean/std of three runs is reported.

Input	Method	F1-score	Accuracy	Precision	Recall	MCC	AUROC	AUPRC
Seq	EMBER	21.07 \pm 1.60	67.86 \pm 1.53	28.37 \pm 2.43	21.91 \pm 1.61	17.41 \pm 2.95	58.89 \pm 2.24	28.88 \pm 0.57
	DeepPhos	17.85 \pm 1.13	65.36 \pm 1.39	18.08 \pm 2.49	20.33 \pm 0.79	1.42 \pm 3.91	47.52 \pm 2.68	20.98 \pm 1.12
	MusiteDeep	16.04 \pm 0.09	66.98 \pm 0.63	13.39 \pm 0.12	20.00 \pm 0.00	0.00 \pm 0.00	46.42 \pm 4.46	20.81 \pm 0.95
	ESM-2	57.40 \pm 1.38	86.79 \pm 1.15	61.57 \pm 2.13	56.47 \pm 0.91	74.26 \pm 2.22	94.91 \pm 1.02	60.80 \pm 2.63
Str	StructGNN	23.90 \pm 3.27	71.45 \pm 1.44	36.40 \pm 4.25	23.87 \pm 2.89	31.60 \pm 2.58	82.25 \pm 0.35	46.12 \pm 2.54
	GraphTrans	20.85 \pm 3.49	68.95 \pm 1.59	29.21 \pm 8.70	22.07 \pm 2.76	21.20 \pm 3.88	75.77 \pm 4.02	36.54 \pm 0.91
	GVP	28.31 \pm 2.32	73.24 \pm 0.62	40.66 \pm 7.84	26.76 \pm 2.02	38.95 \pm 2.08	83.56 \pm 1.69	50.94 \pm 2.95
	PiFold	22.29 \pm 3.10	69.37 \pm 1.27	31.53 \pm 12.39	23.73 \pm 2.00	22.99 \pm 7.39	70.69 \pm 1.53	35.35 \pm 1.15
Seq + Str	GearNet	31.05 \pm 0.26	78.95 \pm 0.75	27.68 \pm 0.25	39.90 \pm 0.00	61.16 \pm 0.82	92.31 \pm 0.90	54.49 \pm 0.78
	CDCConv	45.20 \pm 3.20	81.12 \pm 1.35	47.68 \pm 0.25	51.23 \pm 3.31	66.25 \pm 2.24	92.99 \pm 0.27	56.65 \pm 0.97
	MIND	43.88 \pm 11.54	84.46 \pm 0.54	50.10 \pm 4.11	43.01 \pm 10.99	67.65 \pm 1.68	84.13 \pm 2.31	51.34 \pm 1.19
	MeToken	61.95 \pm 1.07	88.39 \pm 1.04	64.97 \pm 1.14	60.40 \pm 1.17	77.56 \pm 1.44	95.88 \pm 0.52	64.05 \pm 1.19

5.3 ABLATION STUDY

To highlight the impact of components, we compare MeToken against several baseline configurations. The results, as detailed in Table 4, offer a depiction of how each element contributes to the overall effectiveness: (i) Micro-env (Me): This baseline employs an end-to-end model that considers micro-environments without tokenization. Serving as a fundamental benchmark, it attains an F1-score of 40.04%. (ii) Me + Uni-Codebook: By integrating micro-environment tokenization with a uniform sub-codebook that acknowledges the long-tail distribution of PTM types, this configuration yields a substantial enhancement, elevating the F1-score to 48.04%. (iii) Me + TS-VQ: This setup explores the use of an unconstrained codebook paired with temperature-scaled vector quantization (TS-VQ). Despite TS-VQ’s theoretical benefits—softer assignments and broader exploration—this configuration disappointingly results in an F1-score of only 37.46%.

These findings underscore the crucial necessity for a well-structured codebook; in the absence of such a framework, the inherent advantages of TS-VQ cannot be fully realized, particularly when navigating the complexities introduced by the long-tail distribution of PTM types. Ultimately, our comprehensive implementation of MeToken, which synergistically combines micro-environment tokenization with a uniform sub-codebook and TS-VQ, achieves the highest performance, attaining

an impressive F1-score of 50.40%. This result illustrates the effectiveness of our integrated approach in maximizing the model’s potential.

Table 4: The ablation of MeToken on the large-scale dataset.

Method	Accuracy	Precision	Recall	F1-score	MCC	AUROC	AUPRC
Micro-env (Me)	88.82	49.09	37.81	40.04	73.48	91.98	42.95
Me + Uni-Codebook	88.74	51.95	47.70	48.04	73.37	92.32	48.62
Me + TS-VQ	88.22	41.29	38.62	37.46	72.54	91.25	40.51
MeToken	89.91	58.08	47.93	50.40	76.03	92.20	51.26

5.4 VISUALIZATION AND BIOLOGICAL UNDERSTANDING OF OUR MODEL

We visualize the code embeddings learned by MeToken using t-SNE (Van der Maaten & Hinton, 2008) in Figure 6. Due to space constraints, we used abbreviated labels, with their full names available in Appendix G. It reveals three key observations that offer biologically relevant insights:

① **Relationship between different types of Glycosylation:** C-glycosylation is positioned notably far from N- and O-glycosylation. Unlike N- and O-glycosylation, where the sugar attaches to nitrogen (N) or oxygen (O) atoms, C-glycosylation involves the formation of a covalent bond between the sugar and a carbon atom (Ihara et al., 2015; Lovelace et al., 2011). This spatial separation in the embedding space aligns with the fundamental differences in their underlying biochemical mechanisms.

② **Competitive modification between phosphorylation and acetylation sites:** The scattered distribution of phosphorylation and acetylation sites in the plot reflects the competitive nature of these PTMs (Shukri et al., 2023; Csizmok & Forman-Kay, 2018). Both modifications often occur within the same microenvironment and compete for access to nearby residues, resulting in the observed pattern where these two PTMs are dispersed, sometimes adjacent or interleaved.

③ **Distribution of phosphorylation and ubiquitination sites** These sites are distributed in a dispersed manner, lacking a central cluster but instead spread across several distinct regions. This fragmented pattern aligns with observations from previous studies (Shi, 2009)(Johnson & Lewis, 2001)(Johnson, 2009), which emphasize the intricate interplay between these two PTMs. They often function in a coordinated fashion, regulating diverse aspects of protein behavior.

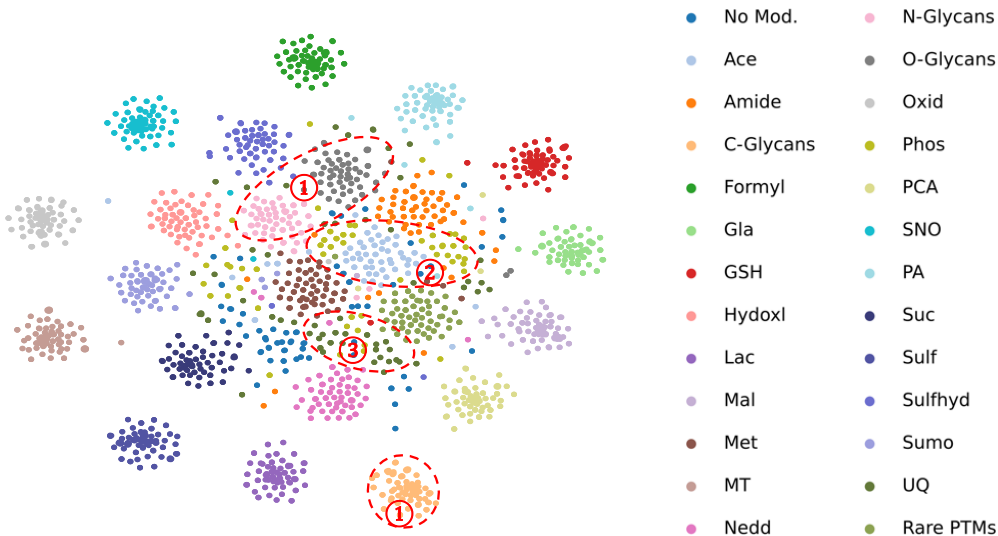


Figure 6: The visualization of the learned codebook.

6 CONCLUSION AND LIMITATION

In this study, we focus on PTM prediction, a fundamental challenge in proteomics research. By constructing a large-scale sequence-structure PTM dataset, we established a robust benchmark. Our MeToken harnesses the power of micro-environment tokenization, utilizing uniform codebook loss and temperature-scaled vector quantization to model the interactions within protein micro-environments for predicting long-tail PTM types. Our results demonstrate that MeToken significantly outperforms state-of-the-art approaches, underscoring the importance of incorporating structural data for a comprehensive understanding of PTM sites. The findings offer a pathway to more precise PTM prediction and enhance our understanding of protein functionality.

Despite its strengths, our study has several limitations. While our dataset is a blend of PDB data and AlphaFold database, it relies predominantly on AlphaFold predictions. This dependence may introduce biases inherent to the AlphaFold model. Furthermore, our model currently does not consider interactions between the protein and other molecules, such as enzymes, ligands, or interacting proteins, which play crucial roles in the natural environment of PTMs. Addressing these limitations will be a primary focus of our future research endeavors.

ACKNOWLEDGEMENTS

This work was supported by National Science and Technology Major Project (No. 2022ZD0115101), National Natural Science Foundation of China Project (No. U21A20427), Project (No. WU2022A009) from the Center of Synthetic Biology and Integrated Bioengineering of Westlake University and Integrated Bioengineering of Westlake University and Project (No. WU2023C019) from the Westlake University Industries of the Future Research Funding.

REFERENCES

- Ernst Bause and Harald Hettkamp. Primary structural requirements for n-glycosylation of peptides in rat liver. *Febs Lett*, 108(2):341–344, 1979.
- Helen M Berman, John Westbrook, Zukang Feng, Gary Gilliland, Talapady N Bhat, Helge Weissig, Ilya N Shindyalov, and Philip E Bourne. The protein data bank. *Nucleic acids research*, 28(1): 235–242, 2000.
- Can Chen, Jingbo Zhou, Fan Wang, Xue Liu, and Dejing Dou. Structure-aware protein self-supervised learning. *Bioinformatics*, 39(4):btad189, 2023.
- Ting Chen, Lala Li, and Yizhou Sun. Differentiable product quantization for end-to-end embedding compression. In *ICML*, pp. 1617–1626. PMLR, 2020.
- International Human Genome Sequencing Consortium. Finishing the euchromatic sequence of the human genome. *Nature*, 431(7011):931–945, 2004.
- Pierrick Craveur, Tarun J Narwani, Joseph Rebehmed, and Alexandre G de Brevern. Investigation of the impact of ptms on the protein backbone conformation. *Amino Acids*, 51(7):1065–1079, 2019.
- Edward R Cruz, Hung Nguyen, Tin Nguyen, and Ian S Wallace. Functional analysis tools for post-translational modification: a post-translational modification database for analysis of proteins and metabolic pathways. *The Plant Journal*, 99(5):1003–1013, 2019.
- Veronika Csizmok and Julie D Forman-Kay. Complex regulatory mechanisms mediated by the interplay of multiple post-translational modifications. *Current opinion in structural biology*, 48: 58–67, 2018.
- Justas Dauparas, Ivan Anishchenko, Nathaniel Bennett, Hua Bai, Robert J Ragotte, Lukas F Milles, Basile IM Wicky, Alexis Courbet, Rob J de Haas, Neville Bethel, et al. Robust deep learning-based protein sequence design using proteinmpnn. *Science*, 378(6615):49–56, 2022.
- Yonathan Lissanu Deribe, Tony Pawson, and Ivan Dikic. Post-translational modifications in signal integration. *Nature structural & molecular biology*, 17(6):666–672, 2010.

- Alaaeldin El-Nouby, Matthew J Muckley, Karen Ullrich, Ivan Laptev, Jakob Verbeek, and Hervé Jégou. Image compression with product quantized masked image modeling. *arXiv preprint arXiv:2212.07372*, 2022.
- Hehe Fan, Zhangyang Wang, Yi Yang, and Mohan Kankanhalli. Continuous-discrete convolution for geometry-sequence modeling in proteins. In *The Eleventh International Conference on Learning Representations*, 2022.
- Jianjiong Gao, Andreas Prlić, Chunxiao Bi, Wolfgang F Bluhm, Dimitris Dimitropoulos, Dong Xu, Philip E Bourne, and Peter W Rose. Biojava-modfinder: identification of protein modifications in 3d structures from the protein data bank. *Bioinformatics*, 33(13):2047–2049, 2017.
- Zhangyang Gao, Cheng Tan, and Stan Z Li. Pifold: Toward effective and efficient protein inverse folding. In *The Eleventh International Conference on Learning Representations*, 2022.
- Zhangyang Gao, Cheng Tan, and Stan Z Li. Foldtoken4: Consistent & hierarchical fold language. *bioRxiv*, pp. 2024–08, 2024.
- Vladimir Gligorijević, P Douglas Renfrew, Tomasz Kosciolk, Julia Koehler Leman, Daniel Berenberg, Tommi Vatanen, Chris Chandler, Bryn C Taylor, Ian M Fisk, Hera Vlamakis, et al. Structure-based protein function prediction using graph convolutional networks. *Nature communications*, 12(1):3168, 2021.
- Douglas Hanahan and Lisa M Coussens. Accessories to the crime: functions of cells recruited to the tumor microenvironment. *Cancer cell*, 21(3):309–322, 2012.
- Pedro Hermosilla, Marco Schäfer, Matej Lang, Gloria Fackelmann, Pere-Pau Vázquez, Barbora Kozlikova, Michael Krone, Tobias Ritschel, and Timo Ropinski. Intrinsic-extrinsic convolution and pooling for learning on 3d protein structures. In *International Conference on Learning Representations*, 2020.
- Xiaokun Hong, Ningshan Li, Jiyang Lv, Yan Zhang, Jing Li, Jian Zhang, and Hai-Feng Chen. Ptmint database of experimentally verified ptm regulation on protein–protein interaction. *Bioinformatics*, 39(1):btac823, 2023.
- Bozhen Hu, Cheng Tan, Jun Xia, Jiangbin Zheng, Yufei Huang, Lirong Wu, Yue Liu, Yongjie Xu, and Stan Z Li. Learning complete protein representation by deep coupling of sequence and structure. *bioRxiv*, pp. 2023–07, 2023.
- Bin Huang, Tingwen Fan, Kaiyue Wang, Haicang Zhang, Chungong Yu, Shuyu Nie, Yangshuo Qi, Wei-Mou Zheng, Jian Han, Zheng Fan, et al. Accurate and efficient protein sequence design through learning concise local environment of residues. *Bioinformatics*, 39(3):btad122, 2023.
- Sean J Humphrey, David E James, and Matthias Mann. Protein phosphorylation: a major switch mechanism for metabolic regulation. *Trends in Endocrinology & Metabolism*, 26(12):676–687, 2015.
- Yoshito Ihara, Yoko Inai, Midori Ikezaki, In Sook L Matsui, Shino Manabe, and Yukishige Ito. C-mannosylation: modification on tryptophan in cellular proteins. In *Glycoscience: biology and medicine*, pp. 1091–1100. Springer Japan, 2015.
- John Ingraham, Vikas Garg, Regina Barzilay, and Tommi Jaakkola. Generative models for graph-based protein design. *Advances in neural information processing systems*, 32, 2019.
- Ole Nørregaard Jensen. Modification-specific proteomics: characterization of post-translational modifications by mass spectrometry. *Current opinion in chemical biology*, 8(1):33–41, 2004.
- Jianhua Jia, Zi Liu, Xuan Xiao, Bingxiang Liu, and Kuo-Chen Chou. isuc-pseopt: identifying lysine succinylation sites in proteins by incorporating sequence-coupling effects into pseudo components and optimizing imbalanced training dataset. *Analytical biochemistry*, 497:48–56, 2016a.
- Jianhua Jia, Zi Liu, Xuan Xiao, Bingxiang Liu, and Kuo-Chen Chou. psuc-lys: predict lysine succinylation sites in proteins with pseaac and ensemble random forest approach. *Journal of theoretical biology*, 394:223–230, 2016b.

- Wengong Jin, Regina Barzilay, and Tommi Jaakkola. Hierarchical generation of molecular graphs using structural motifs. In *International conference on machine learning*, pp. 4839–4848. PMLR, 2020.
- Bowen Jing, Stephan Eismann, Patricia Suriana, Raphael John Lamarre Townshend, and Ron Dror. Learning from protein structure with geometric vector perceptrons. In *International Conference on Learning Representations*, 2020.
- Louise N Johnson. The regulation of protein phosphorylation. *Biochemical Society Transactions*, 37(4):627–641, 2009.
- Louise N Johnson and Richard J Lewis. Structural basis for control by phosphorylation. *Chemical reviews*, 101(8):2209–2242, 2001.
- Biing-Hwang Juang and A Gray. Multiple stage vector quantization for speech coding. In *ICASSP*, pp. 597–600. IEEE, 1982.
- Herve Jégou, Matthijs Douze, and Cordelia Schmid. Product quantization for nearest neighbor search. *IEEE Transactions on Pattern Analysis and Machine Intelligence*, 33(1):117–128, 2011. doi: 10.1109/TPAMI.2010.57.
- Kathryn E Kirchoff and Shawn M Gomez. Ember: multi-label prediction of kinase-substrate phosphorylation events through deep learning. *Bioinformatics*, 38(8):2119–2126, 2022.
- Xiangzhe Kong, Wenbing Huang, and Yang Liu. Conditional antibody design as 3d equivariant graph translation. In *The Eleventh International Conference on Learning Representations*, 2023a. URL <https://openreview.net/forum?id=LFHFQbjxIiP>.
- Xiangzhe Kong, Wenbing Huang, and Yang Liu. End-to-end full-atom antibody design. In *International Conference on Machine Learning*, pp. 17409–17429. PMLR, 2023b.
- Doyup Lee, Chiheon Kim, Saehoon Kim, Minsu Cho, and Wook-Shin Han. Autoregressive image generation using residual quantization. In *CVPR*, pp. 11523–11532, 2022.
- Tzong-Yi Lee, Yi-Ju Chen, Tsung-Cheng Lu, Hsien-Da Huang, and Yu-Ju Chen. Snsite: exploiting maximal dependence decomposition to identify cysteine s-nitrosylation with substrate site specificity. *PLoS one*, 6(7):e21849, 2011.
- Fuyi Li, Cunshuo Fan, Tatiana T Marquez-Lago, André Leier, Jerico Revote, Cangzhi Jia, Yan Zhu, A Ian Smith, Geoffrey I Webb, Quanzhong Liu, et al. Prismoid: a comprehensive 3d structure database for post-translational modifications and mutations with functional impact. *Briefings in bioinformatics*, 21(3):1069–1079, 2020.
- Songling Li, Hong Li, Mingfa Li, Yu Shyr, Lu Xie, and Yixue Li. Improved prediction of lysine acetylation by support vector machines. *Protein and peptide letters*, 16(8):977–983, 2009.
- Wen Li, Feifei Li, Xia Zhang, Hui-Kuan Lin, and Chuan Xu. Insights into the post-translational modification and its emerging role in shaping the tumor microenvironment. *Signal transduction and targeted therapy*, 6(1):422, 2021.
- Zhengyi Li, Menglu Li, Lida Zhu, and Wen Zhang. Improving ptm site prediction by coupling of multi-granularity structure and multi-scale sequence representation. *arXiv preprint arXiv:2401.10211*, 2024.
- Zhongyan Li, Shangfu Li, Mengqi Luo, Jih-Hua Jhong, Wenshuo Li, Lantian Yao, Yuxuan Pang, Zhuo Wang, Rulan Wang, Renfei Ma, et al. dbptm in 2022: an updated database for exploring regulatory networks and functional associations of protein post-translational modifications. *Nucleic acids research*, 50(D1):D471–D479, 2022a.
- Zutan Li, Jingya Fang, Shining Wang, Liangyun Zhang, Yuanyuan Chen, and Cong Pian. Adapt-kr: a novel deep learning framework for accurate prediction of lysine crotonylation sites based on learning embedding features and attention architecture. *Briefings in Bioinformatics*, 23(2):bbac037, 2022b.

- Zeming Lin, Halil Akin, Roshan Rao, Brian Hie, Zhongkai Zhu, Wenting Lu, Nikita Smetanin, Robert Verkuil, Ori Kabeli, Yaniv Shmueli, et al. Evolutionary-scale prediction of atomic-level protein structure with a language model. *Science*, 379(6637):1123–1130, 2023.
- Yaning Liu, Zhaomin Yu, Cheng Chen, Yu Han, and Bin Yu. Prediction of protein crotonylation sites through lightgbm classifier based on smote and elastic net. *Analytical biochemistry*, 609:113903, 2020.
- Leslie L Lovelace, Christopher L Cooper, James M Sodetz, and Lukasz Lebioda. Structure of human c8 protein provides mechanistic insight into membrane pore formation by complement. *Journal of Biological Chemistry*, 286(20):17585–17592, 2011.
- Hongyuan Lu, Daniel J Diaz, Natalie J Czarnecki, Congzhi Zhu, Wantae Kim, Raghav Shroff, Daniel J Acosta, Bradley R Alexander, Hannah O Cole, Yan Zhang, et al. Machine learning-aided engineering of hydrolases for pet depolymerization. *Nature*, 604(7907):662–667, 2022.
- Fenglin Luo, Minghui Wang, Yu Liu, Xing-Ming Zhao, and Ao Li. Deepphos: prediction of protein phosphorylation sites with deep learning. *Bioinformatics*, 35(16):2766–2773, 2019.
- Shitong Luo, Yufeng Su, Xingang Peng, Sheng Wang, Jian Peng, and Jianzhu Ma. Antigen-specific antibody design and optimization with diffusion-based generative models for protein structures. In *Advances in Neural Information Processing Systems*, 2022.
- Hao Lv, Fu-Ying Dao, Zheng-Xing Guan, Hui Yang, Yan-Wen Li, and Hao Lin. Deep-kcr: accurate detection of lysine crotonylation sites using deep learning method. *Briefings in bioinformatics*, 22(4):bbaa255, 2021.
- Julieta Martinez, Holger H Hoos, and James J Little. Stacked quantizers for compositional vector compression. *arXiv preprint arXiv:1411.2173*, 2014.
- Lingkuan Meng, Wai-Sum Chan, Lei Huang, Linjing Liu, Xingjian Chen, Weitong Zhang, Fuzhou Wang, Ke Cheng, Hongyan Sun, and Ka-Chun Wong. Mini-review: Recent advances in post-translational modification site prediction based on deep learning. *Computational and Structural Biotechnology Journal*, 20:3522–3532, 2022.
- Fabian Mentzer, David Minnen, Eirikur Agustsson, and Michael Tschannen. Finite scalar quantization: Vq-vae made simple. *arXiv preprint arXiv:2309.15505*, 2023.
- Viet Thanh Duy Nguyen and Truong Son Hy. Multimodal pretraining for unsupervised protein representation learning. *Biology Methods and Protocols*, 9(1), 2024.
- Wang-Ren Qiu, Bi-Qian Sun, Hua Tang, Jian Huang, and Hao Lin. Identify and analysis crotonylation sites in histone by using support vector machines. *Artificial intelligence in medicine*, 83:75–81, 2017.
- Yigong Shi. Serine/threonine phosphatases: mechanism through structure. *Cell*, 139(3):468–484, 2009.
- Ali H Shukri, Valentina Lukinović, François Charih, and Kyle K Biggar. Unraveling the battle for lysine: A review of the competition among post-translational modifications. *Biochimica et Biophysica Acta (BBA)-Gene Regulatory Mechanisms*, pp. 194990, 2023.
- Martin Steinegger and Johannes Söding. Mmseqs2 enables sensitive protein sequence searching for the analysis of massive data sets. *Nature biotechnology*, 35(11):1026–1028, 2017.
- Cheng Tan, Zhangyang Gao, Lirong Wu, Jun Xia, Jiangbin Zheng, Xihong Yang, Yue Liu, Bozhen Hu, and Stan Z Li. Cross-gate mlp with protein complex invariant embedding is a one-shot antibody designer. In *Proceedings of the AAAI Conference on Artificial Intelligence*, volume 38, pp. 15222–15230, 2024.
- Niraj Thapa, Meenal Chaudhari, Sean McManus, Kaushik Roy, Robert H Newman, Hiroto Saigo, and Dukka B Kc. Deepsuccinylsite: a deep learning based approach for protein succinylation site prediction. *BMC bioinformatics*, 21:1–10, 2020.

- Dimitrios Tsikas. Post-translational modifications (ptm): analytical approaches, signaling, physiology and pathophysiology—part i. *Amino Acids*, 53(4):485–487, 2021.
- Aaron Van Den Oord, Oriol Vinyals, et al. Neural discrete representation learning. *Advances in neural information processing systems*, 30, 2017.
- Laurens Van der Maaten and Geoffrey Hinton. Visualizing data using t-sne. *Journal of machine learning research*, 9(11), 2008.
- Mihaly Varadi, Stephen Anyango, Mandar Deshpande, Sreenath Nair, Cindy Natassia, Galabina Yordanova, David Yuan, Oana Stroe, Gemma Wood, Agata Laydon, et al. Alphafold protein structure database: massively expanding the structural coverage of protein-sequence space with high-accuracy models. *Nucleic acids research*, 50(D1):D439–D444, 2022.
- Mihaly Varadi, Damian Bertoni, Paulyna Magana, Urmila Paramval, Ivanna Pidruchna, Malarvizhi Radhakrishnan, Maxim Tsenkov, Sreenath Nair, Milot Mirdita, Jingi Yeo, et al. Alphafold protein structure database in 2024: providing structure coverage for over 214 million protein sequences. *Nucleic Acids Research*, 52(D1):D368–D375, 2024.
- Christopher T Walsh, Sylvie Garneau-Tsodikova, and Gregory J Gatto Jr. Protein posttranslational modifications: the chemistry of proteome diversifications. *Angewandte Chemie International Edition*, 44(45):7342–7372, 2005.
- Gary Walsh and Roy Jefferis. Post-translational modifications in the context of therapeutic proteins. *Nature biotechnology*, 24(10):1241–1252, 2006.
- Duolin Wang, Shuai Zeng, Chunhui Xu, Wangren Qiu, Yanchun Liang, Trupti Joshi, and Dong Xu. Musitedeep: a deep-learning framework for general and kinase-specific phosphorylation site prediction. *Bioinformatics*, 33(24):3909–3916, 2017.
- Limei Wang, Haoran Liu, Yi Liu, Jerry Kurtin, and Shuiwang Ji. Learning hierarchical protein representations via complete 3d graph networks. In *The Eleventh International Conference on Learning Representations*, 2022.
- Zichen Wang, Steven A Combs, Ryan Brand, Miguel Romero Calvo, Panpan Xu, George Price, Nataliya Golovach, Emmanuel O Salawu, Colby J Wise, Sri Priya Ponnappalli, et al. Lm-gvp: A generalizable deep learning framework for protein property prediction from sequence and structure. *bioRxiv*, pp. 2021–09, 2021.
- Jacob West-Roberts, Joshua Kravitz, Nishant Jha, Andre Cornman, and Yunha Hwang. Diverse genomic embedding benchmark for functional evaluation across the tree of life. *bioRxiv*, pp. 2024–07, 2024.
- Lirong Wu, Yijun Tian, Yufei Huang, Siyuan Li, Haitao Lin, Nitesh V Chawla, and Stan Z Li. Mapeppi: Towards effective and efficient protein-protein interaction prediction via microenvironment-aware protein embedding. *arXiv preprint arXiv:2402.14391*, 2024.
- Jun Xia, Chengshuai Zhao, Bozhen Hu, Zhangyang Gao, Cheng Tan, Yue Liu, Siyuan Li, and Stan Z Li. Mole-bert: Rethinking pre-training graph neural networks for molecules. In *The Eleventh International Conference on Learning Representations*, 2022.
- Yubin Xie, Xiaotong Luo, Yupeng Li, Li Chen, Wenbin Ma, Junjiu Huang, Jun Cui, Yong Zhao, Yu Xue, Zhixiang Zuo, et al. Deepnitro: prediction of protein nitration and nitrosylation sites by deep learning. *Genomics, Proteomics and Bioinformatics*, 16(4):294–306, 2018.
- Yu Xue, Ao Li, Lirong Wang, Huanqing Feng, and Xuebiao Yao. Ppsp: prediction of pk-specific phosphorylation site with bayesian decision theory. *BMC bioinformatics*, 7:1–12, 2006.
- Yu Xue, Zexian Liu, Xinjiao Gao, Changjiang Jin, Longping Wen, Xuebiao Yao, and Jian Ren. Gps-sno: computational prediction of protein s-nitrosylation sites with a modified gps algorithm. *PLoS one*, 5(6):e11290, 2010.

- Yu Yan, Jyun-Yu Jiang, Mingzhou Fu, Ding Wang, Alexander R Pelletier, Dibakar Sigdel, Dominic CM Ng, Wei Wang, and Peipei Ping. Mind-s is a deep-learning prediction model for elucidating protein post-translational modifications in human diseases. *Cell reports methods*, 3(3), 2023.
- Kai Yu, Ye Wang, Yongqiang Zheng, Zekun Liu, Qingfeng Zhang, Siyu Wang, Qi Zhao, Xiaolong Zhang, Xiaoxing Li, Rui-Hua Xu, et al. qptm: an updated database for ptm dynamics in human, mouse, rat and yeast. *Nucleic Acids Research*, 51(D1):D479–D487, 2023a.
- Lijun Yu, José Lezama, Nitesh B Gundavarapu, Luca Versari, Kihyuk Sohn, David Minnen, Yong Cheng, Agrim Gupta, Xiuye Gu, Alexander G Hauptmann, et al. Language model beats diffusion-tokenizer is key to visual generation. *arXiv preprint arXiv:2310.05737*, 2023b.
- Neil Zeghidour, Alejandro Luebs, Ahmed Omran, Jan Skoglund, and Marco Tagliasacchi. Soundstream: An end-to-end neural audio codec. *IEEE/ACM Transactions on Audio, Speech, and Language Processing*, 30:495–507, 2021.
- Zuobai Zhang, Minghao Xu, Arian Rokkum Jamasb, Vijil Chenthamarakshan, Aurelie Lozano, Payel Das, and Jian Tang. Protein representation learning by geometric structure pretraining. In *The Eleventh International Conference on Learning Representations*, 2022.

A CODEBOOK SUPPRESSES THE IMPACT OF LONG-TAIL DISTRIBUTION

The ‘‘long-tail distribution’’ issue refers to the phenomenon where a small number of PTM types are highly prevalent, while many others are rare. From an engineering perspective, this issue necessitates a solution that ensures all PTM types, including the rare ones, are adequately represented in the model’s learning process. This led us to the development of the sub-codebook strategy in our MeToken model. The engineering solutions can be summarized as follows:

Uniform representation By allocating an identical size sub-codebook to each PTM type, we ensure that rare PTMs have as much representation as others. This uniform distribution of codebooks prevents the model from being dominated by frequent PTMs, promoting a balanced learning process.

Strong discrimination Each sub-codebook is designed to capture distinct patterns specific to its corresponding PTM type. This focused representation allows the model to learn more precise and discriminative features for each PTM type. By ensuring that each PTM type has its own dedicated sub-codebook, the model can better differentiate between various types, improving its ability to identify and predict even the rarest PTMs accurately.

In summary, the sub-codebook strategy addresses the long-tail distribution issue by providing a balanced and discriminative representation for all PTM types, thereby enhancing the model’s overall performance and reliability in PTM prediction.

B NODE AND EDGE EMBEDDING

Following (Gao et al., 2022), we implement the initial node and edge embeddings for the protein graph with manually constructed structural features. As shown in Table 5, this comprehensive encoding captures the intricate local structural information inherent in each residue of a protein, facilitating a detailed representation crucial for our PTM prediction tasks.

Table 5: The initial node and edge embeddings.

Level	Feature	Illustration
Intra-residue Node	Angle	$\{ \sin, \cos \} \times \{ \alpha_i, \beta_i, \gamma_i, \phi_i, \psi_i, \omega_i \}$
	Distance	$\left\{ \text{RBF}(\ \omega_i - C\alpha_i\) \mid \omega \in \{C, N, O\} \right\}$
	Direction	$\left\{ \mathbf{Q}_i^T \frac{\omega_i - C\alpha_i}{\ \omega_i - C\alpha_i\ } \mid \omega \in \{C, N, O\} \right\}$
Inter-residue Edge	Orientation	$\mathbf{q}(\mathbf{Q}_i^T \mathbf{Q}_j)$
	Distance	$\left\{ \text{RBF}(\ \omega_i - \omega_j\) \mid j \in \mathcal{N}(i), \omega \in \{C_\alpha, C, N, O\} \right\}$
	Direction	$\left\{ \mathbf{Q}_i^T \frac{\omega_i - \omega_j}{\ \omega_i - \omega_j\ } \mid j \in \mathcal{N}(i), \omega \in \{C_\alpha, C, N, O\} \right\}$

Specifically, the node embeddings incorporate a variety of geometric and structural characteristics that provide a comprehensive view of each residue’s local environment: (i) angle features, such as α_i (angle for $N_i-C\alpha_i-C_i$), β_i (angle for $C_{i-1}-N_i-C\alpha_i$), γ_i (angle for $C\alpha_i-C_i-N_{i+1}$), ϕ_i (dihedral angle for $N_i-C\alpha_i$), ψ_i (dihedral angle for $C-C\alpha_i$), and ω_i (dihedral angle for C_i-N_i). (ii) distance features, where we employ radial basis functions (RBFs) to transform distances between backbone atoms and the central $C\alpha_i$ atom into features, capturing the relative positioning of significant structural elements within each residue. (iii) direction features, which are defined by the local coordinate system \mathbf{Q}_i and the normalized vectors pointing from the $C\alpha_i$ atom to the C, N, O atoms.

Edge embeddings focus on characterizing the interactions between adjacent residues, crucial for understanding how proteins fold and function: (i) orientation features, where $\mathbf{q}(\cdot)$ is the quaternions of relative rotation between the local coordinate systems of two residues. (ii) distance features, which

capture the distances between the backbone atoms of two residues, transformed into radial basis functions. (iii) direction features, which are defined by projecting the normalized vectors between backbone atoms of neighboring residues onto the local coordinate systems Q_i . In our model, the micro-environments of each residue are defined through a comprehensive approach that considers three distinct types of neighbor atom sets. Specifically, the neighborhoods denoted as $\mathcal{N}(i)$ are categorized based on three criteria: sequential order, K-nearest neighbors, and R-radius proximity.

C DATASET CONSTRUCTION

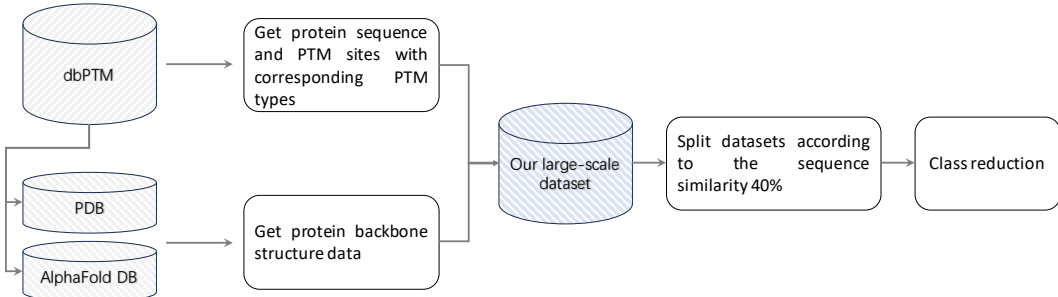


Figure 7: The data processing pipeline for constructing our large-scale PTM dataset.

As illustrated in Figure 7, our dataset construction process was designed to compile a comprehensive and robust resource for investigating post-translational modifications (PTMs) across a wide array of protein types. We began by selecting dbPTM as our foundational sequence-based dataset, which is highly regarded for its extensive catalog of PTM types, encompassing a rich variety of biochemical modifications. In order to enrich this sequence information with structural data, we sourced corresponding structural information from two primary repositories: the Protein Data Bank (PDB) and the AlphaFold database. Our protocol prioritizes experimental data from PDB; however, in instances where such data is unavailable, we resort to high-confidence predictions from AlphaFold, ensuring both accuracy and completeness in our structural dataset representation. Following Dauparas et al. (2022), we introduced Gaussian noise with a mean of zero and a standard deviation of 0.0005 to the atomic coordinates. The addition of this noise simulates small structural fluctuations and uncertainties that may occur in real-world experimental conditions, thereby improving the generalization ability of models trained on our data.

To ensure the integrity of our training and evaluation process and to prevent data leakage, we employed MMseqs2 (Steinegger & Söding, 2017), a highly efficient software suite for handling large biological sequence data through clustering. We clustered the raw data based on sequence similarity, setting a stringent threshold to ensure that proteins in the validation and test sets exhibit no more than 40% similarity to those in the training set. This split provides a reliable measure of performance.

Addressing the challenge of sample imbalance—a common issue in PTM datasets where modified sites are significantly outnumbered by unmodified sites, and some types of modifications are substantially rarer than others. As shown in Figure 8, we consolidated PTM types with fewer than 100 samples into a single ‘rare sites’ category. We reduced the 73 classes, which included a ‘No modification’ class to 26 classes. This new classification framework comprises 24 distinct PTM classes, one aggregated class for rare modifications, and one class representing the absence of modification.

In Table 6, we present a comparative analysis between our dataset and other open-sourced PTM datasets. Our dataset contains 1,263,935 PTM sites across 187,812 proteins, offering a detailed exploration of 72 types of modifications. This not only encapsulates a broader diversity of PTM types than typically available but also includes a significantly larger number of protein entries, establishing it as an unparalleled resource in the field. Notably, unlike other datasets such as dbPTM and qPTM, our dataset integrates both sequence and structural data for each protein entry. This integration is crucial for developing more accurate and predictive models of PTM sites, as the structural context often influences where and how modifications occur. Our dataset not only bridges the gap in the availability of comprehensive sequence-structure PTM data but also sets a new standard for the scale and scope of such resources. It enables advanced modeling techniques that can exploit detailed structural contexts alongside sequence information, paving the way for breakthroughs in understanding the complex mechanisms of post-translational modifications.

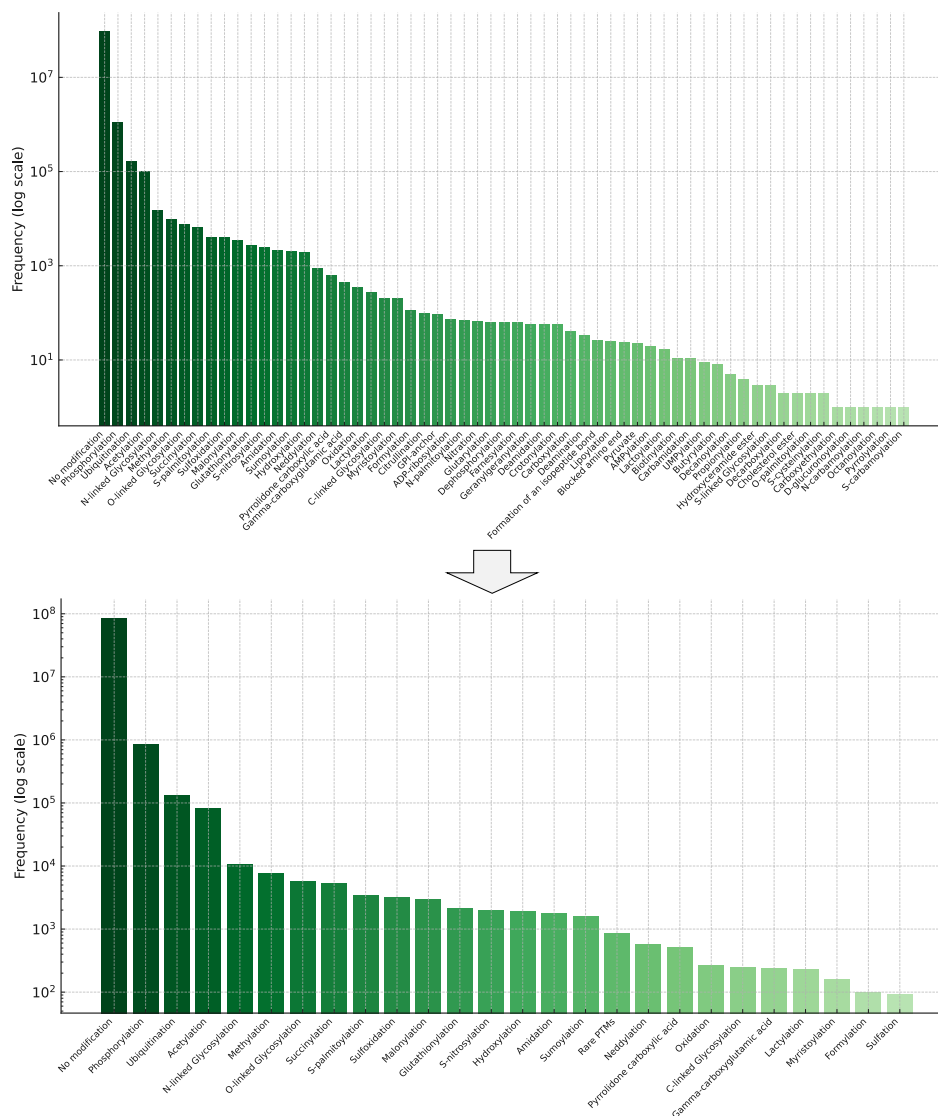


Figure 8: The distribution of PTM classes after class reduction.

The PTMint dataset is a relatively modest collection of 2,477 samples spanning 1,169 proteins with six PTM types. The qPTM dataset offers a broader scope, encompassing 660,030 samples across 40,728 proteins, also classified into the six PTM types. These PTM types are consistent with a subset from our large-scale dataset. Originally, the qPTM dataset lacked comprehensive structural information, which prompted us to enhance it by integrating structural data retrieved from the AlphaFold database.

Table 6: The comparison between open-sourced PTM datasets with our large-scale dataset.

Database	Number of sites	Number of proteins	Modification types	Sequence	Structure
PTMint	2,477	1,169	6	✓	✓
PTM Structure	11,677	3,828	21	✓	✓
PRISMOID	17,145	3,919	37	✓	✓
qPTM	660,030	40,728	6	✓	✗
dbPTM	2,235,000	223,678	72	✓	✗
Ours	1,263,935	187,812	72	✓	✓

D METRICS

To comprehensively evaluate the performance of the PTM prediction task, which we regard as a multi-class classification problem, we adopted a robust suite of metrics. These metrics include accuracy, precision, recall, F1-score, the Matthews Correlation Coefficient (MCC), the Area Under the Receiver Operating Characteristic curve (AUROC), and the Area Under the Precision-Recall Curve (AUPRC). Each of these metrics offers distinct insights into the model’s performance, from overall accuracy to the balance between sensitivity and specificity.

Accuracy provides a straightforward measure of the overall correctness of the predictions across all classes. It is calculated as the ratio of correctly predicted observations to the total observations:

$$\text{Accuracy} = \frac{\sum_{i=1}^N \mathbb{1}(y_i = \hat{y}_i)}{N}, \quad (8)$$

where y_i is the true PTM type, \hat{y}_i is the predicted PTM type, and N is the total number of instances.

Precision (macro) measures the accuracy of positive predictions. It is especially critical in datasets where false positives carry a significant cost:

$$\text{Precision} = \frac{1}{K} \sum_{k=1}^K \frac{\text{TP}_k}{\text{TP}_k + \text{FP}_k}, \quad (9)$$

where TP_k and FP_k are the true positives and false positives for the k -class, respectively, and K is the total number of classes.

Recall (macro) assesses the model’s ability to correctly identify all relevant instances per class:

$$\text{Recall} = \frac{1}{K} \sum_{k=1}^K \frac{\text{TP}_k}{\text{TP}_k + \text{FN}_k}, \quad (10)$$

where FN_k are the false negatives for the k -class.

F1-score (macro) is the harmonic mean of precision and recall for each class:

$$\text{F1-score} = \frac{1}{K} \sum_{k=1}^K \frac{2 \times \text{Precision}_k \times \text{Recall}_k}{\text{Precision}_k + \text{Recall}_k}. \quad (11)$$

Matthews Correlation Coefficient (MCC) takes into account true and false positives and negatives and is generally regarded as a balanced measure that can be used even if the classes are of very different sizes:

$$\text{MCC} = \frac{1}{K} \sum_{k=1}^K \frac{\text{TP}_k \times \text{TN}_k - \text{FP}_k \times \text{FN}_k}{\sqrt{(\text{TP}_k + \text{FP}_k) \times (\text{TP}_k + \text{FN}_k) \times (\text{TN}_k + \text{FP}_k) \times (\text{TN}_k + \text{FN}_k)}}, \quad (12)$$

Area Under the Receiver Operating Characteristic curve (AUROC) evaluates the trade-off between true positive rate and false positive rate, providing an aggregate measure of performance across all classification thresholds. It reflects the model’s ability to discriminate between classes:

$$\text{AUROC} = \frac{1}{K} \sum_{k=1}^K \text{AUROC}_k, \quad (13)$$

where AUROC_k is the AUROC for the k -class, defined by integrating the TPR over the range of possible values of FPR:

$$\text{AUROC}_k = \int_0^1 \text{TPR}_k(\text{FPR}_k) d\text{FPR}_k, \quad (14)$$

and $\text{TPR}_k = \text{TP}_k / (\text{TP}_k + \text{FN}_k)$ and $\text{FPR}_k = \text{FP}_k / (\text{TN}_k + \text{FP}_k)$ are the true positive rate and false positive rate for the k -class, respectively.

Area Under the Precision-Recall Curve (AUPRC) assesses the trade-off between Precision and Recall for a given class at various threshold levels, which is particularly useful when dealing with imbalanced datasets:

$$\text{AUPRC} = \frac{1}{K} \sum_{k=1}^K \text{AUPRC}_k. \quad (15)$$

where AUPRC_k is the AUPRC for the k -class, defined as:

$$\text{AUPRC}_k = \int_0^1 \text{Precision}_k(\text{Recall}_k) d\text{Recall}_k. \quad (16)$$

E IMPLEMENTATION DETAILS

We provide detailed implementation information for the models evaluated in our study. These models are categorized into sequence-based, structure-based, and sequence-structure models, each designed to predict PTM sites based on different data modalities.

E.1 SEQUENCE-BASED MODELS

DeepPhos As shown in Figure 9, this model (Luo et al., 2019) is composed of densely connected convolutional neural network (DC-CNN) blocks, designed to capture multiple representations of sequences for the final phosphorylation prediction. Specifically, the DC-CNN block operates as a multi-scale pyramid-like merging structure, adept at extracting features from diverse perspectives. Although it aims to predict phosphorylation sites, we adapt the model to predict other PTM types by modifying the output layer to accommodate the desired PTM classes.

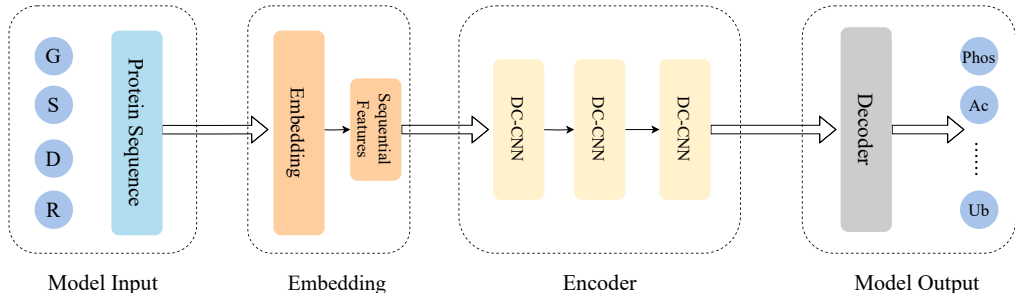


Figure 9: The model architecture of DeepPhos.

EMBER As shown in Figure 10, EMBER(Kirchoff & Gomez, 2022) employs a modified Siamese neural network tailored for multi-label prediction tasks to generate high-dimensional embeddings of motif vectors. Additionally, it uses one-hot encoded motif sequences and leverages these two distinct representations as dual inputs into the classifier.

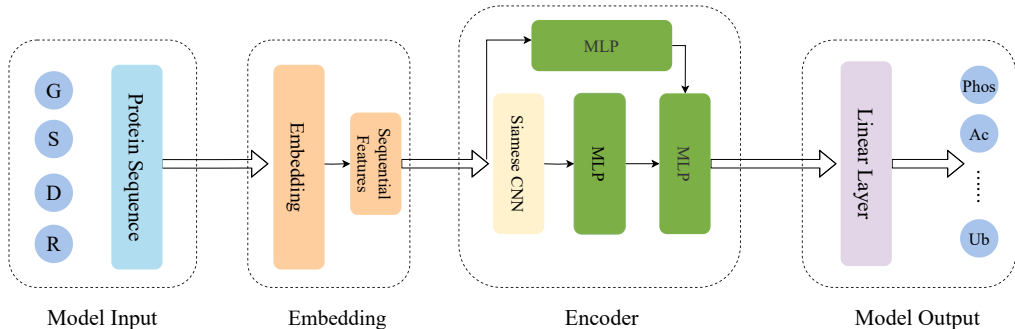


Figure 10: The model architecture of EMBER.

MusiteDeep As shown in Figure 11, Multi-layer CNN is used as the feature extractor but no pooling layers are used. The last hidden state of multi-layer CNN is copied twice, where one directly inputs into the attention mechanism and the other first trans-positioned and then inputs into another attention mechanism. The output of the two attention layer mechanisms is combined and input into the fully connected neural network layers. The final layer is a single layer with the softmax output.

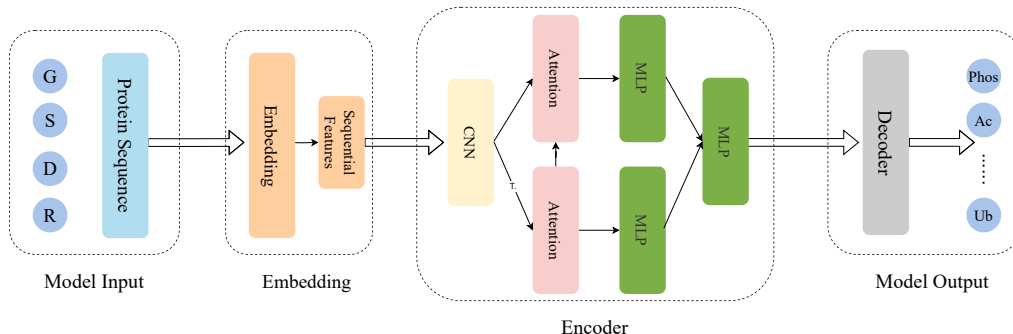


Figure 11: The model architecture of MusiteDeep.

ESM As shown in Figure 12, we utilize the pretrained model from ESM (Lin et al., 2023) to obtain embeddings of protein sequences. These embeddings serve as a rich representation of the protein data, capturing intricate evolutionary patterns. Following this, an MLP is employed as the classifier.

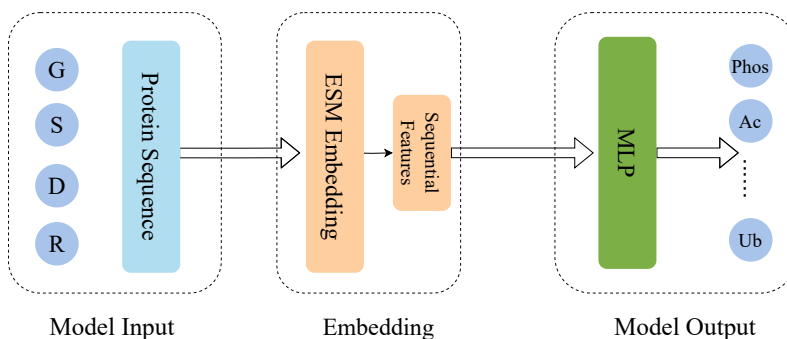


Figure 12: The model architecture of ESM.

E.2 STRUCTURE-BASED MODELS

StructGNN As shown in Figure 13, StructGNN (Ingraham et al., 2019) is a traditional protein design model that has been adapted in this work to predict residue-level post-translational modification (PTM) sites. The model begins by obtaining structural features through a conventional structure embedding process. These features capture the intricate three-dimensional configurations of protein structures. Following this, the model employs layers of a Message Passing Neural Network, which iteratively refines the structural representations by aggregating information across the network.

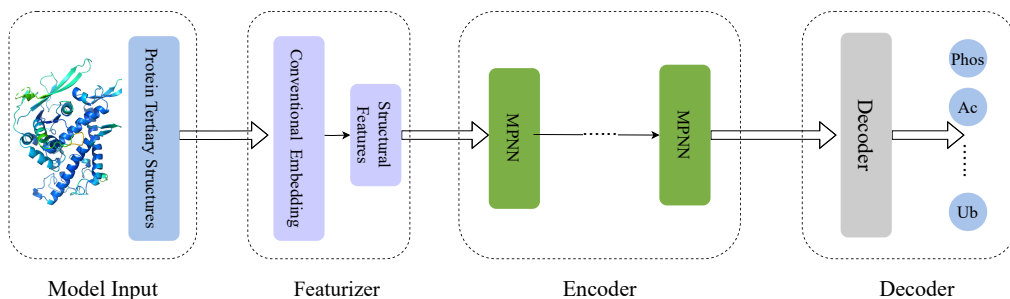


Figure 13: The model architecture of StructGNN.

GraphTrans Figure 14 shows that GraphTrans (Ingraham et al., 2019) is a Transformer-based model that replaces StructGNN’s MPNN layers with attention mechanisms. This modification allows the model to capture long-range dependencies and intricate interactions within the protein structure more effectively.

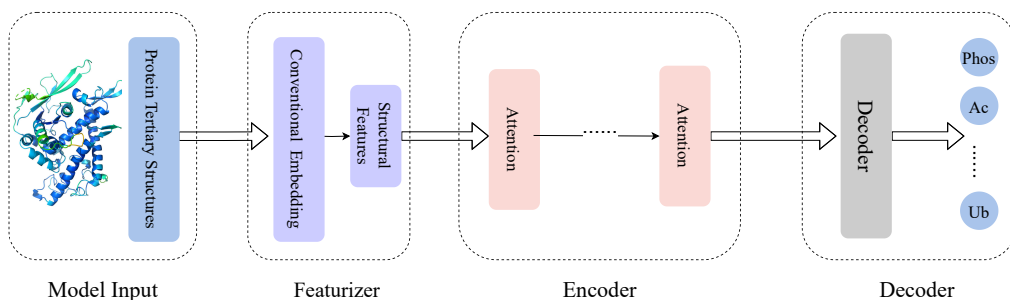


Figure 14: The model architecture of GraphTrans

GVP GVP (Jing et al., 2020) introduce geometric vector perceptrons, which extend standard dense layers to operate on collections of Euclidean vectors. Graph neural networks equipped with such layers are able to perform both geometric and relational reasoning on efficient representations of macromolecules.

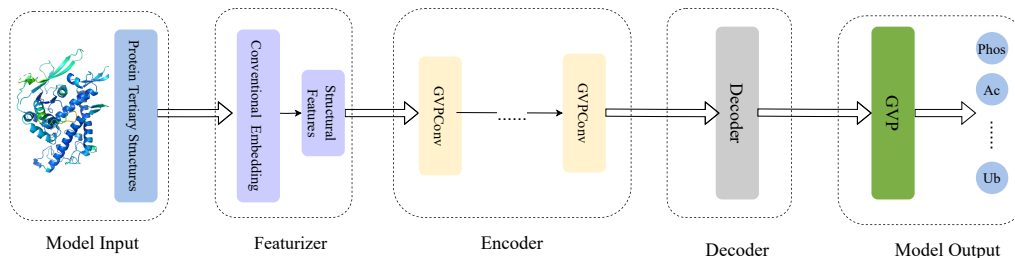


Figure 15: The model architecture of GVP.

PiFold This model extracts features of protein structures and employs a sophisticated encoder-decoder architecture. The featurizer module leverages virtual atoms to enhance the representation of spatial information, capturing critical characteristics such as distances, angles, and directions. PiGNN that tailored for protein structure representation to encode structural features and MLP as a decoder.

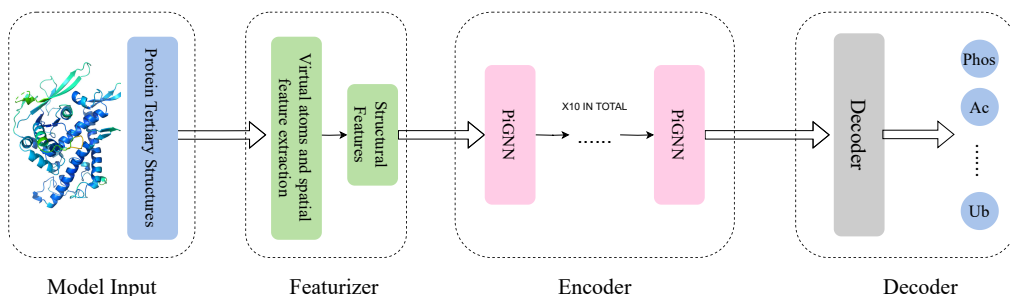


Figure 16: The model architecture of PiFold.

E.3 SEQUENCE-STRUCTURE MODELS

GearNet As depicted in Figure 17, GearNet (Zhang et al., 2022)—the Geometry-Aware Relational Graph Neural Network—is a simple yet highly effective structure-based protein encoder. GearNet

encodes spatial information by incorporating various types of sequential and structural edges into the protein residue graphs. It then performs relational message passing, allowing the model to capture and integrate complex spatial relationships within the protein structure.

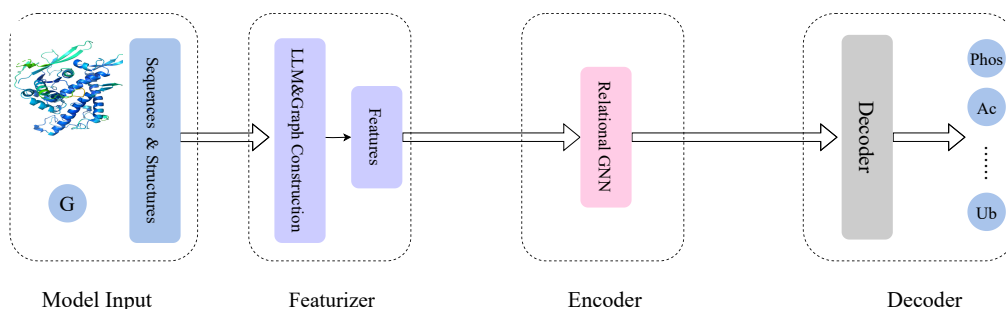


Figure 17: The model architecture of GearNet.

CDConv As illustrated in Figure 18, the Continuous-Discrete Convolution (CDConv) is introduced to simultaneously model the geometry and sequence structures of proteins using distinct approaches for their regular and irregular characteristics. CDConv employs independent learnable weights to handle regular sequential displacements within the protein sequence. For the irregular geometric displacements, it directly encodes these variations to capture the complex spatial relationships inherent in the protein's three-dimensional structure.

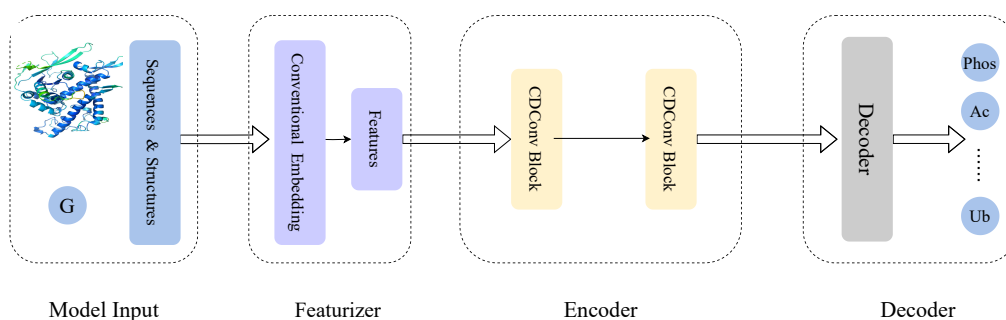


Figure 18: The model architecture of CDConv.

MIND As illustrated in Figure 19, the MIND model employs a dual-path approach to analyze protein data. One path leverages LSTM networks combined with attention mechanisms to scrutinize the sequence information. The other path constructs the protein structure as a graph and utilizes graph attention mechanisms to analyze the structural data. A MLP then integrates the information from both paths, functioning as a classifier to make final predictions.

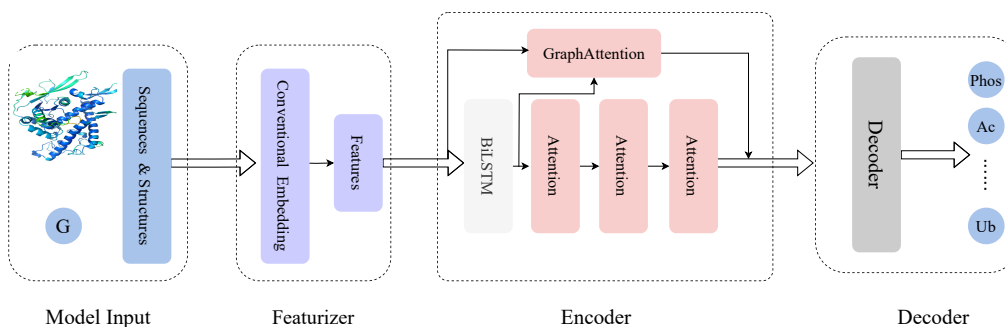


Figure 19: The model architecture of MIND.

F SUPPLEMENTARY EXPERIMENTS

F.1 ESM-3 BASELINE

In our investigation, we also examined the performance of the ESM-3 model, as shown in Table 7. Surprisingly, our results indicated that fine-tuning ESM-2 outperforms fine-tuning ESM-3 in this context. Previous research (West-Roberts et al., 2024) has suggested that ESM-3 does not consistently outperform ESM-2, highlighting an intriguing nuance in model performance. One potential explanation for this phenomenon is that ESM-3 incorporates considerations of sequence, structure, and function, which may introduce a level of complexity that does not always lead to enhanced performance for specific tasks like PTM prediction.

Table 7: Performance comparison between ESM-2 and ESM-3 models.

Method	F1	Acc	Pre	Rec	MCC	AUROC	AUPRC
ESM2	43.94	89.75	55.67	42.15	75.83	91.52	47.31
ESM3	40.65	87.48	45.72	38.67	70.31	89.91	41.36

F.2 OTHER SEQUENCE-STRUCTURE BASELINES

We also conducted experiments using additional sequence-structure models to further contextualize our findings, as shown in Table 8. The STEPS model (Chen et al., 2023) structures data as a graph and utilizes sequence language models for embedding sequences, focusing on maximizing the mutual information between sequence and structure through a pseudo bi-level optimization approach. However, unlike MeToken, which is specifically designed for residue-level tasks, STEPS is tailored primarily for protein-level applications, limiting its effectiveness in our targeted analysis. Similarly, MPRL (Nguyen & Hy, 2024) adopts a multimodal framework that integrates ESM-2 for sequence embedding, alongside VGAE and point cloud techniques for structure embedding, culminating in a fusion module that generates a comprehensive representative embedding. While MPRL demonstrates strong performance in protein-level tasks, it struggles to adequately address the nuances of residue-level tasks, revealing a gap in its applicability. The results indicate that both STEPS and MPRL, while effective in their respective domains, demonstrate limitations when applied to residue-level tasks, further emphasizing the unique capabilities of MeToken in this PTM prediction.

Table 8: Performance metrics for STEPS and MPRL models.

Method	F1	Acc	Pre	Rec	MCC	AUROC	AUPRC
STEPS	15.96	66.32	13.26	20.04	2.80	41.72	19.69
MPRL	19.04	90.39	18.08	20.11	5.02	52.68	21.55

F.3 THE RELIABILITY OF ALPHAFOLD2’S PREDICTED DATA

To assess the reliability of our large-scale dataset, we conducted a thorough validation analysis in Table 9. The combination of AlphaFold2 predictions and PDB data produced the highest performance metrics, highlighting the importance of combining predicted and experimental structures. Specifically, the AF2-only dataset demonstrated significantly lower performance, revealing the limitations inherent in relying solely on predictions. In contrast, the PDB-only dataset outperformed AF2, yet it still did not match the performance of the hybrid AF2+PDB dataset. This indicates that while experimental data plays a critical role, the extensive scale of AF2 predictions substantially enhances overall results.

Table 9: Performance metrics across different datasets.

Dataset	F1	Acc	Pre	Rec	MCC	AUROC	AUPRC
AF2+PDB	50.40	89.91	58.08	47.93	76.03	92.20	51.26
AF2	11.74	87.23	10.29	14.80	54.54	41.79	12.95
PDB	41.31	73.39	40.96	47.10	52.25	91.07	40.87

These findings suggest that, although AF2 data may introduce certain biases, its large scale contributes positively to performance. Ultimately, the most effective outcomes arise from integrating both predicted and experimental data, achieving an optimal balance between scale and accuracy. This analysis reinforces the conclusion that the integration of AF2 predictions with PDB data not only mitigates potential biases but also maximizes predictive power, thereby enhancing the reliability of our large-scale dataset and its applicability in protein research.

F.4 STATISTICS ABOUT CODEBOOK DISTRIBUTION

To illustrate the distribution of tokens within our codebook, we examine a specific token with index 2588. As depicted in Figure 20, the most prevalent amino acids associated with this token are valine (Val, V) and leucine (Leu, L), both of which are hydrophobic amino acids characterized by similar structural properties. The other three amino acids in the distribution are also hydrophobic, reinforcing this trend. This observation indicates that our model has effectively learned and captured significant physicochemical features of amino acids within the codebook. Such a finding enhances the credibility and interpretability of our model, demonstrating its ability to reflect meaningful biological properties in its decent representations.

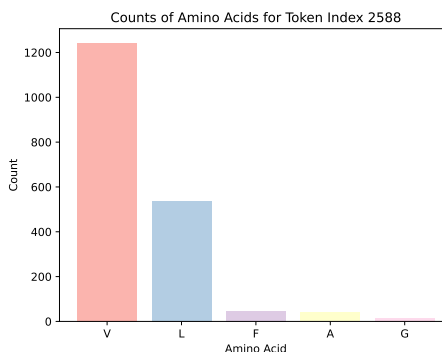


Figure 20: The corresponding amino acid distribution of the token 2588.

G ABBREVIATIONS OF PTMS

Due to space constraints, we have used abbreviations in some places in the main text for PTMs. Below is the table of abbreviations and their corresponding full names.

Table 10: Abbreviations and corresponding names of PTMs.

Abbreviation	PTM types
Ac	Acetylation
Amide	Amidation
C-Glycans	C-linked Glycosylation
Formyl	Formylation
Gla	Gamma-carboxyglutamic acid
GSH	Glutathionylation
Hydroxyl	Hydroxylation
Lac	Lactylation
Mal	Malonylation
Met	Methylation
MT	Myristoylation
Nedd	Neddylation
N-Glycans	N-linked Glycosylation
O-Glycan	O-linked Glycosylation
Oxid	Oxidation
Phos	Phosphorylation
PCA	Pyrrolidone carboxylic acid
SNO	S-nitrosylation
PA	S-palmitoylation
Suc	Succinylation
Sulf	Sulfation
Sulhyd	Sulfoxidation
Sumo	Sumoylation
Ub	Ubiquitination